# Nanoscale palladium-on-gold catalysis for glycerol oxidation

*Study of the catalytic performance as a function of palladium surface coverage and the stability of the catalyst structure as a function of catalyst size*

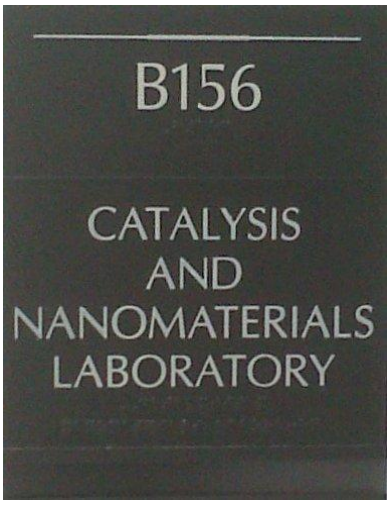


**Author:**

J. Arentz – University of Groningen – Student number S1843559

**Supervisors:**

Prof. dr. A. A. Broekhuis – University of Groningen

Prof. dr. ir. H.J. Heeres – University of Groningen

Prof. M. S. Wong – Rice University

RuG

RICE

**Chemical Reaction Engineering Group**

*University of Groningen*

**August 2012**

# Nanoscale palladium-on-gold catalysis for glycerol oxidation

*Study of the catalytic performance as a function of palladium surface coverage and the stability of the catalyst structure as a function of catalyst size*

**THESIS SUBMITTED**
**IN FULFILLMENT OF THE**
**REQUIREMENTS FOR THE DEGREE**
**Master of Science**
**(Chemical Engineering)**


**Author:**

Joni Arentz
(joniarentz@hotmail.com)

**Supervisors:**

Prof. dr. A. A. (Ton) Broekhuis
(a.a.broekhuis@rug.nl)

Prof. dr. ir. H.J. (Hero Jan) Heeres
(h.j.heeres@rug.nl)

Prof. Michael (Mike) S. Wong
(mswong@rice.edu)

**Chemical Reaction Engineering Group**
*University of Groningen*


**August 2012**

# Abstract

This thesis covers the work carried out during an exploratory study into the use of a supported palladium-covered gold catalyst for the aqueous phase oxidation of glycerol under mild reaction conditions. The study was initiated by combining the following triggers: 1. glycerol is experiencing a global glut due to the massive production of biodiesel and the price drop of crude and refined glycerol. There is a high need to actuate practical avenues for converting glycerol into value-added products, 2. Available knowledge regarding the use of palladium, platinum or gold-based catalysts for the oxidation of glycerol, and 3. Positive experiences with a palladium-covered gold-based catalyst in the conversion of perchloroethylene and trichloroethene present in groundwater.

This palladium-on-gold catalyst offers a potential to convert glycerol into more economically valuable products like glyceric acid, lactic acid and tartronic acid. Also, the feasibility of this catalytic technology can be improved by re-designing the catalyst in order to increase catalytic activity. Insight in the nanoscale palladium-on-gold catalyst and the mechanism of reaction is gained. Research is performed in two parts; Part I describes a Pd surface coverage study and part II describes a catalyst size study. In part I monometallic Au and Pd supported catalysts and a series of carbon supported Pd on Au (Pd/Au) catalysts with different Pd surface coverages ranging from 10% to 300% were prepared and used in the liquid phase oxidation of glycerol in water using oxygen as the oxidant. Systematic investigation of catalytic activity with alternate Pd surface coverages on support in the selective oxidation of glycerol has not yet been reported. Catalytic activity and selectivity were found to be a function of surface coverage of the shell Pd atoms on the core Au atoms, with the highest activity and selectivity detected at ~60% and ~100% respectively. A 98.1% conversion of glycerol was observed at a 60% Pd surface coverage, in just 3 hours time. It is hypothesized that the reactivity order for metal species is $Pd^0 > Au^0 > Pd^{2+}$ and that Au has a unique ability to stabilize surface Pd atoms in metallic form that is resistant to experimental conditions (pH 13.6, 60 °C, and $O_2$ flow). A reaction mechanism has been proposed for the glycerol oxidation using Pd/Au catalysts to explain the formation of all observed compounds. In part II Pd/Au nanoparticles with a core diameter of ~3, ~7 and ~10 nm with a Pd loading of 60% were prepared and characterized by EXAFS. The composition and atomic-scale structure of the catalysts before, during and after the liquid phase oxidation of glycerol in water using oxygen as the oxidant, are reported. From the small change in Fourier transforms, the corresponding bond distances, the Debye-Waller Factor of 0.0 and the almost completely constant coordination numbers, it can be concluded that the structure of Pd/Au nanoparticles holds for different core diameters and remains intact during the aqueous-phase selective oxidation of glycerol.

This catalyst provides a potential way to convert glycerol into more economically valuable products.

# Table of Contents

# List of Tables

# List of Figures

# 1 Introduction

This report covers the work carried out during an exploratory study into the use of a supported palladium-covered gold catalyst (palladium-on-gold deposited on active carbon) for the oxidation of glycerol under mild reaction conditions. The following introduction will present an overall outline of the study including some background regarding the triggers that led to this work. Next the overall research plan will be presented.

The research project was initiated by combining the following triggers:

1. The large scale glycerol availability as by-product of the biodiesel industry which results in the need to develop pathways to add value to this feedstock.
   In general, from every 100 kg biodiesel produced, approximately 10 kg of crude glycerol will be left as a waste compound which has limited economic value [1]. Due to the massive production of biodiesel, glycerol, known to man as the oldest organic molecule in life form, is experiencing a global glut. To tackle the global glycerol glut, a substantial amount of research activities has been undertaken worldwide to identify attractive transformations to convert glycerol into more valuable compounds (elaborated in Chapter 1.3).
2. Available knowledge regarding the use of palladium, platinum or gold-based catalysts for the oxidation of glycerol.
   In the selective oxidation [1]of glycerol, gold is shown to be effective as a catalyst [2]. In the liquid-phase oxidation of glycerol, platinum catalysts gave valuable oxidation products such as glyceric acid or dihydroxyacetone. Also, a high selectivity to glyceric acid (77% at 90% conversion) can be obtained by air oxidation of glycerol solutions on palladium catalysts [3]. However, for bimetallic Pd-Au catalysts significant improvements in the activity and selectivity have been observed with respect to monometallic systems [2, 4] (elaborated in Chapter 1.4).
3. Positive experiences with a palladium-covered gold catalyst in the conversion of perchloroethylene and trichloroethene present in groundwater.
   The catalysis and nanomaterials group at Rice University have widely studied palladium-on-gold catalysts in the application of groundwater remediation [5, 6-11]. It has been demonstrated that the palladium-on-gold nanoparticles can catalyze the hydrodechlorination reactions of perchloroethylene and trichloroethene, under mild reaction conditions (room temperature, atmospheric pressure) (elaborated in Chapter 1.5).

**The aim/objective** of this study follows from the combination of these three triggers and may be defined as: screening and optimization of nanosized supported palladium-on-gold catalysts in the oxidative conversion of glycerol to value-added chemicals.

The three triggers and aim of this study lead to the **hypothesis:** palladium-on-gold nanoparticles could be partially effective for the oxidation of glycerol to value-added chemicals, if not fully due to an oxidative environment.

In this study, insight is gained in the nanoscale palladium-on-gold catalyst and reaction mechanism and kinetics of glycerol and its components in selective oxidation reactions. Part I covers the results of supported palladium-on-gold catalysts with varying palladium surface coverages for glycerol oxidation (in collaboration with Mr. Z. Zhao).

[1] Selective oxidation is a reaction carried out in the presence of a catalyst under controlled conditions to maximize the formation of the desired product.

Part II describes the stability in atomic-scale structure of supported palladium-on-gold catalysts with different core diameters during the aqueous-phase selective oxidation of glycerol (in collaboration with Ms. L. Pretzer).

## *1.1 Goals of research*

This thesis deals with the upgrading of glycerol to glyceric acid by aqueous phase selective oxidation mediated with a supported Pd-on-Au catalyst.
The feasibility of this catalytic technology can be improved by re-designing the Pd material in order to increase catalytic activity. Insight in the nanoscale Pd-on-Au catalyst and the mechanism of reaction is also gained.

In Part I, palladium-on-gold nanoparticles with a core diameter of ~4 nm with different palladium loadings are synthesized and characterized by HPLC.
Bimetallic palladium-on-gold catalysts have shown significant improvements in the activity and selectivity for the oxidation of glycerol.
Also, for the hydrodechlorination of trichloroethylene and perchloroethylene, the highest rates were found with ~4 nm palladium-on-gold nanoparticles at a 60-80% palladium surface coverage. The hydrodechlorination reactions were performed under mild reaction conditions (room temperature, atmospheric pressure). For a typical selective oxidation reaction of glycerol, mild conditions are also used (60 oC, 0.12 L/min O2 flow).
This leads to the **hypothesis** that the unique ability of Pd-on-Au to catalyze the hydrodechlorination reactions of perchloroethylene and trichloroethene should partially hold for the glycerol oxidation reaction. With the highest activity expected at 70-80% Pd surface coverage [9].

In Part II, Pd/Au nanoparticles with a core diameter of ~3, ~7 and ~10 nm with a Pd loading of 60% are synthesized and characterized by EXAFS. The aim is to test the stability of the catalyst structure as a function of catalyst size.
**Hypothesis**: the structure of Pd/Au nanoparticles [5] holds for different core diameters and remains intact during the aqueous-phase selective oxidation of glycerol.

Research plan:

- Literature study on glycerol oxidation
- Investigate the applicability of the Pd-on-Au catalyst, which has been used successfully for groundwater remediation by Wong *et al.*, for the oxidation of glycerol
- Study the reaction mechanism for the Pd-on-Au catalyst with different Pd surface coverages
- Study the kinetics of this 1$^{st}$ order glycerol oxidation
- Propose an overall reaction mechanism
- Study the effect of the catalyst structure (different core diameters) on catalyst stability

## *1.2 Detailed research plan*

To gain insight in the reaction mechanisms, the corresponding kinetics and the catalyst structure, experiments are conducted. The research was comprised of several phases in order to accomplish the hypotheses and goals set above:

- Literature study
  - Selective oxidation of glycerol
  - Initial studies with respect to the Pd/Au supported on activated carbon (AC) catalysts
  - Modelling and kinetics

- Experimental
  - Pd surface coverage study
    - Catalyst preparation
      - Preparation of ~4 nm AC supported Au, Pd & Pd/Au catalysts by sodium citrate-tannic acid reduction method
    - Experiments with various Pd surface coverages in a semi-batch reactor
      - Ranges: 60 °C -0.12 L/min $O_2$
      - Detection method: HPLC
  - Catalyst size study
    - Catalyst preparation
      - Preparation of ~3, ~7 and ~10 nm AC supported Pd/Au catalysts by sodium citrate-tannic acid reduction method
    - Experiments with various core diameters in a semi-batch reactor
      - Ranges: 60 °C -0.12 L/min $O_2$
      - Detection method: EXAFS

- Results
  - Determine the reaction rate constants and kinetics of glycerol oxidation reaction using Pd-on-Au catalysts
  - Ascertain the concentration profiles
  - Determine conversions & selectivities
  - Propose a reaction mechanism
  - Confirm stability of catalysts structure

## *1.3 Glycerol*

Glycerol (1,2,3-Propanetriol) is a colourless, odourless, low toxic, viscous liquid with a sweet taste. The name glycerol stems from the Greek word *glykeros* which means "sweet". In 1779 the Swedish chemist Carl W. Scheele firstly identified glycerol by heating olive oil with lead oxide. Scheele also noticed that the syrupy liquid is completely soluble in water and alcohols [12]. Glycerol's solubility is because it has three hydroxyl groups (Figure 1) which have a tendency to form hydrogen bonds.

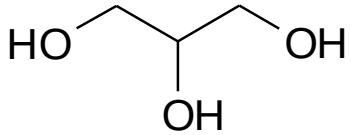


***Figure 1: Structure of glycerol***

In literature, other names, such as glycerine, glycerin, etc., can be found in use interchangeably. However, glycerine and glycerin generally refer to a commercial solution of glycerol in water while glycerol refers to the pure substance.
Glycerol in its pure condition is a liquid at room temperature having the following physical–chemical properties and characteristics (Table 1), which have been obtained from various reference sources.

***Table 1: Summary of the physico-chemical properties of (pure) glycerol at 20 °C***

| Physical property | Value |
|---|---|
| Chemical formula | $C_3H_8O_3$ |
| Molecular mass | 92.09 g $mol^{-1}$ |
| Relative density | 1.261 g/$cm^3$ |
| Viscosity | 1.410 Pa.s |
| Melting Point | 18.2 °C |
| Boiling point | 290 °C at 1013 hPa |
| Flash point | 160 °C (closed cup) |
| Surface tension | 63.4 mN/m |

### 1.3.1 Production & economic aspects

Although glycerol was formerly found as a by-product in soap making, the large scale production of synthetic glycerol from propene began in the 1940s [12]. Nowadays, glycerol is produced in the manufacturing or refining of several chemicals from petroleum and biodiesel to soap. Glycerol obtained as a by-product in the conversion of fatty acid methyl esters (biodiesel), is known as natural or native glycerol. Production of glycerol through other methods like the fermentation of sugar or the hydrogenation of carbohydrates, are not industrially important. The fastest growing source of glycerol is the production of fatty acid methyl esters for biodiesel. Biodiesel is traditionally manufactured by a transesterification reaction between vegetable oil and methanol, catalyzed by a base. This is an equilibrium reaction with the following stoichiometry (Figure 2):

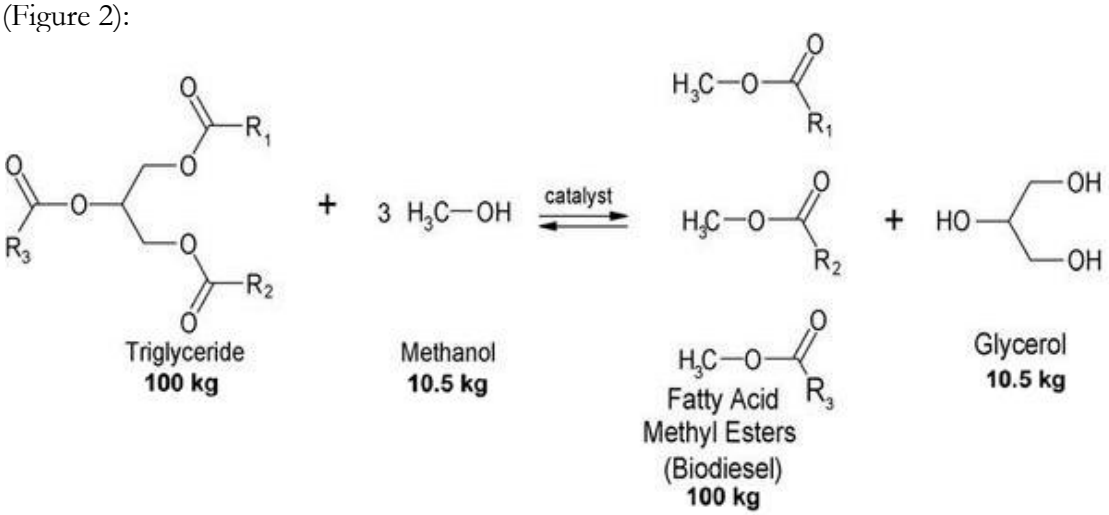


***Figure 2: Transesterification of a triglyceride with methanol***

In general, from every 100 kg biodiesel produced, approximately 10.5 kg glycerol will be left as a by-product [1].
Environmental concerns and possible future shortages have boosted research on alternatives for fossil derived liquid transportation fuels [1]. Biomass is considered a

promising alternative. In recent years, biodiesel as an alternative fuel has attracted increasing interest worldwide [13], leading to a vast increase in production (Figure 3).

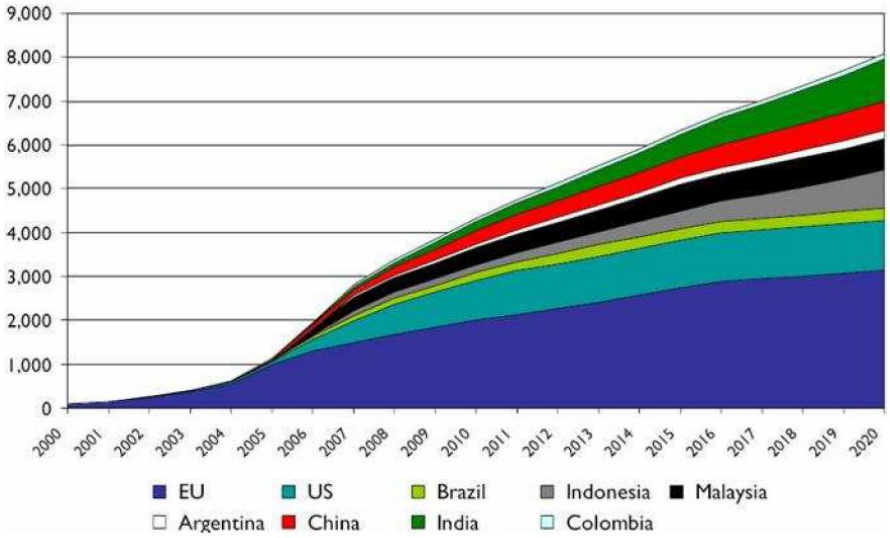


***Figure 3: Estimated biodiesel production by country in million gallons (Source: Promar International)***

There has been an oversupply of glycerol in the world market since 1995 and the increasing production of biodiesel increases the oversupply further. By 2020 the production is estimated to be six times more than the demand [12]. The massive production of biodiesel has also resulted in a dramatic price drop for both crude and refined glycerol. From 2001 to 2006, the price for crude glycerol in the U.S. dropped from $0.20/lb. to less than $0.04/lb., while the price for refined glycerol dropped from more than $0.70/lb. to less than $0.30/lb (Figure 4).

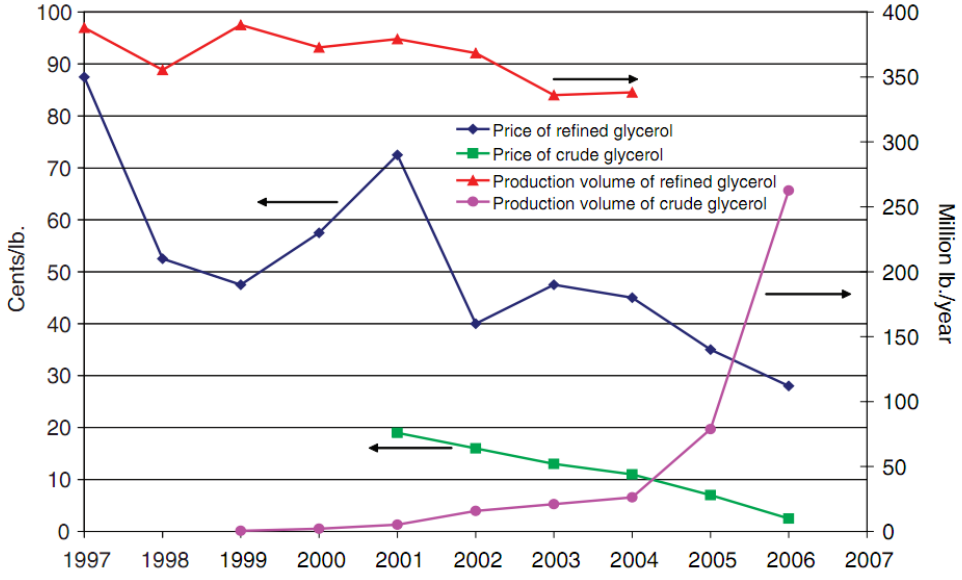


***Figure 4: Market prices and production volumes for refined and crude glycerol (Source: Emerging markets online & national biodiesel board)***

Also, high transportation costs limit glycerol demand. At times the freighting cost is higher than the value of domestic crude glycerol.

Glycerol is experiencing a global glut due to the increasing production of biodiesel, the high transportation costs and price drop of crude & refined glycerol. It is clearly evident

that there is simply more glycerol then the market can handle, which is a significant global issue. A combat against the global glycerol glut is crucial.

### 1.3.2 Conversion

The increasing oversupply of glycerol has lead to tragic measures. As a result, glycerol is being added to animal feed, sprayed onto dirt roads to keep the dust down and even used as landfill [14]. However, to tackle the global glycerol glut, efforts worldwide are being employed to actuate practical avenues for converting glycerol into value-added products. Glycerol has an enormous potential as a versatile feedstock for the production of a wide range of industrially important chemicals (Appendix A).

In summary, glycerol can be converted through:

- Reforming → $H_2$, hydrocarbon fuels [15, 16]
- Dehydration → acrolein, acrylic acid [17, 18]
- Chlorination → dichloropropanol, epichlorohydrin [19]
- Etherification → mono-, di-, tri-tert-butyl esthers, polyglycerols [20]
- Esterification → glycerol carbonate, monoglyceride, diacylglycerol [21]
- Selective reduction → 1,2-propanediol, 1,3-propanediol [22]
- Selective oxidation → glyceric acid, dihydroxyacetone, tartronic acid, oxalic acid, mesoxalic acid, etc. [2]

Of all the processes above, selective oxidation of glycerol is being given special importance due to the introduction of extra functional groups such as carbonyl and carboxylic groups. The valorisation of glycerol during the selective oxidation reaction can also be reflected by the dramatic price increase of the chemicals derived (Figure 5). The current market price for refined glycerol is approximately \$0.05/g. This is lower than almost all of the possible products and much lower than the two major compounds – glyceric acid (\$102/g) and tartronic acid (\$357/g). Note that the prices (in Figure 5) are derived from Sigma Aldrich (a supplier of small quantities of laboratory grade chemicals). Prices of chemicals delivered in bulk quantities will be significantly lower.

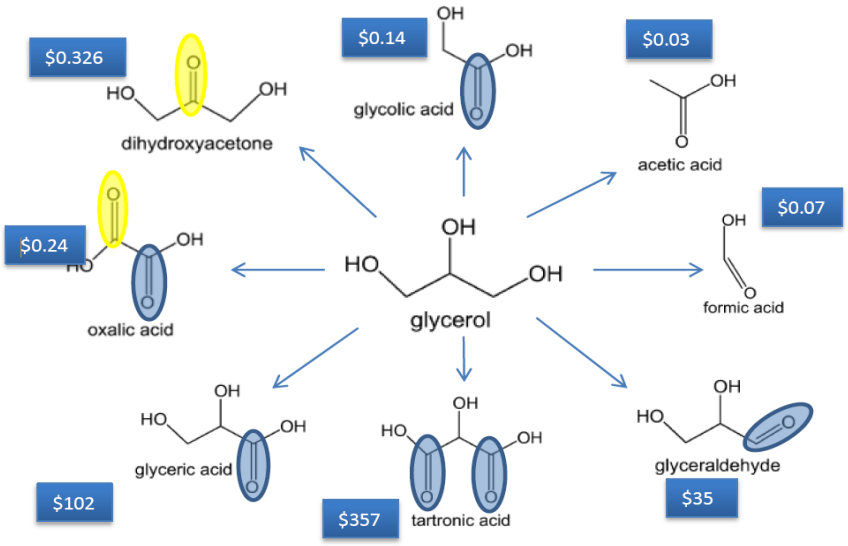


***Figure 5: Chemicals derived from selective oxidation of glycerol and their prices in USD per gram (prices according to [www.sigmaaldrich.com](http://www.sigmaaldrich.com) based on the largest available quantity)***

By oxidizing one primary hydroxyl group (blue colored), glycerol can be converted to glyceraldehydes and glyceric acid. By oxidizing two sides, tartronic acid can be obtained. By selectively oxidizing the secondary OH group (yellow colored), dihydroxyacetone can be formed. Glycerol maintains its $C_3$ structure while being converted to the compounds above. However, $C_2$ compounds such as glycolic acid, oxalic acid and acetic acid are reported to be formed due to the carbon skeleton rupture and rearrangement [23]. $C_1$ in the form of formic acid can be detected in noticeable amounts, while the rest of the $C_1$ compounds exist in $CO_2$ captured by the basic solution (under most experimental conditions).

With the prices for crude and refined glycerol constantly decreasing, the selective oxidation of glycerol to more valuable compounds can diminish the problem of the glycerol glut. Since glycerol can lead to the formation of profitable compounds, control of the selectivity of product is crucial.

## *1.4 Catalyst promoted selective oxidation of glycerol*

Over the last 20 years, the selective oxidation reaction of glycerol has been extensively studied using mainly supported noble metal nanoparticles, such as Pt, Pd and Au using $O_2$ or air as oxidant [3, 24-27].

### 1.4.1 Catalysis

In 1836, Jöns Jakob Berzelius first used the word 'catalysis' in a paper [28], a word that he coined from the Greek *kata* and *lyein* meaning "wholly" and "to loosen" [2929]. A catalyst is a substance that increases the rate of a process without being consumed by the reaction itself.
More than 80% of all existing industrial scale processes rely on catalysis. Many major industrial chemicals and fine chemicals are prepared with the aid of catalysts because:

- it reduces the cost of production (catalysts can be re-used)
- it leads to better selectivity and less waste

Why use a nanosized catalyst?
Nanoparticles have a large surface to volume ratio, which results in a greater contact area between the active material of the catalyst and the surrounding materials. This ensures that the catalyst is used effectively and makes using nanoparticles a major advantage when it comes to designing catalysts. A disadvantage in using nanoparticles is that it is hard to analyze and nanotechnology van be very expensive. However, due to the rapid technological advancements this technology has becomes more accessible.

### 1.4.2 Gold as catalyst

Gold has traditionally been considered to be catalytically inactive [30].
Bond *et al.* are the first to report supported gold catalysts used successfully in the hydrogenation of olefins in 1973 [31]. More than a decade later, Haruta and Hutchings verified gold to be an extraordinary good catalyst [32, 33].

Although gold is the noblest of metals [343231], it is active as a heterogeneous catalyst in both gas and liquid phase. The water/Au interface provides a reaction environment that enhances its catalytic performance [35], used in oxidation, hydrogenation and reduction

reactions. Over the last two decades there has been a dramatic growth of activity in the area of gold catalysis, with the most intensively studied reaction being that of selective oxidation.

### 1.4.3 Selective oxidation with gold catalysts

In recent years interest in gold catalysts for liquid phase oxidation has increased. Supported gold catalysts have been found to be particularly effective for the oxidation of alcohols [36]. Haruta *et al.* demonstrated that gold catalysts can be used in the oxidation of CO as well as in the oxidation of propene [32, 37]. In 2002 Rossi's group reported the application of gold catalysts to the liquid phase oxidation of organic molecules containing carbon oxygen bonds [38]. In 2002 Hutchings and co-workers showed gold to be effective as a catalyst in the selective oxidation of glycerol [2].

### 1.4.4 Selective oxidation of glycerol

The selective oxidation of glycerol using supported Pd and Pt catalysts has been widely investigated by Kimura's and Gallezot's groups [3, 25-27]. In their early studies, Pd was found to be more selective to glyceric acid than Pt with 77% selectivity at 90% conversion [3]. However, bismuth (Bi) promoted Pt was more selective than Pd in converting glycerol to dihydroxyacetone with 70-80% selectivity [26]. Nevertheless, both Pd and Pt suffer deactivation from oxygen poisoning, resulting in relatively low activities [39]. From this earlier work it can be concluded that when the desired product is glyceric acid, Pd is preferred. However, possible deactivation due to oxygen poisoning should be taken into account.

### 1.4.5 Monometallic catalyst

There are only a few studies dedicated to the catalytic activity of unsupported Au sols for liquid-phase reactions. Rossi *et al.* claimed that unsupported Au nanoparticles can be used as a successful catalyst for the aerobic oxidation of glucose. However, the nanoparticles were unstable under the operating conditions. In fact, the gold clusters showed a very short lifetime prior to aggregation, which limits their application as reusable catalysts [40]. Davis and co-workers investigated Au particles with mean sizes ranging from 5 to 42 nm and unsupported Au powder as catalysts in the aqueous-phase oxidation of CO and glycerol. The TOF for the 5 nm Au nanoparticles was higher than that for the large (42 nm) supported Au and bulk Au in the aqueous-phase oxidation of CO. During the aqueous-phase oxidation of glycerol, unsupported Au powder had similar rates and selectivities as those associated with monodispersed 20 and 45 nm supported Au particles. Evidently, 20 nm particles function the same as bulk Au [41].
Also, when using supported catalysts in the aqueous-phase oxidation of glycerol there is a smaller chance in pollution of the HPLC-column as larger particles are more practical to remove from a (liquid) sample.

Recent work from Prati *et al.* has shown that the selective oxidation of mono alcohols and diols with a supported Au catalyst is feasible under mild conditions [42-44]. Inspired by this finding, Hutchings *et al.* extended the work by applying gold catalysts in the selective oxidation of glycerol. They are the first to report Au being active in this reaction [2, 45]. The catalysts used were prepared by reducing an aqueous solution of $HAuCL_4$ with formaldehyde in the presence of a support. By carefully controlling the experimental conditions, 100% selectivity towards glyceric acid was achieved with a 1% Au/AC

catalyst (Table 2). However, the yield is merely 56% which means that 34% of the glycerol has not been converted. To make this catalyst suitable for industrial applications, further work is required.

***Table 2: Oxidation of glycerol using 1% Au/C catalysts [2]***

**Table 1** Oxidation of glycerol using 1% Au/C catalysts[a]

| Catalyst | Glycerol/ mmol | $pO_2$/bar | Glycerol/metal mol ratio | NaOH mmol | Glycerol conversion (%) | Selectivity (%) | | |
|---|---|---|---|---|---|---|---|---|
| | | | | | | Glyceric acid | Glyceraldehyde | Tartronic acid |
| 1% Au/activated carbon 12 | 12 | 3 | 538[b] | 12 | 56 | 100 | 0 | 0 |
| 1% Au/graphite | 12 | 3 | 538[b] | 12 | 54 | 100 | 0 | 0 |
| 1% Au/graphite | 12 | 6 | 538[b] | 12 | 72 | 86 | 2 | 12 |
| 1% Au/graphite | 12 | 6 | 538[b] | 24 | 58 | 97 | 0 | 3 |
| 1% Au/graphite | 6 | 3 | 540[c] | 12 | 56 | 93 | 0 | 7 |
| 1% Au/graphite | 6 | 3 | 540[c] | 6 | 43 | 80 | 0 | 20 |
| 1% Au/graphite | 6 | 3 | 214[d] | 6 | 59 | 63 | 0 | 12 |
| 1% Au/graphite | 6 | 3 | 214[d] | 12 | 69 | 82 | 0 | 18 |
| 1% Au/graphite | 6 | 6 | 214[d] | 6 | 58 | 67 | 0 | 33 |
| 1% Au/graphite | 6 | 6 | 214[d] | 12 | 91 | 92 | 0 | 6 |
| 1% Au/graphite | 6 | 6 | 214[d] | 0 | 0 | | | |
| 5% Pt/activated carbon | 12 | 3 | 500 | 12 | 63 | 74 | 21 | 0 |
| 5% Pt/activated carbon | 12 | 3 | 500 | 24 | 56 | 69 | 30 | 0 |
| 5% Pt/activated carbon | 6 | 6 | 100 | 12 | 88 | 55 | 0 | 23 |

[a] *Reaction conditions*: 60 °C, 3 h, $H_2O$ (and 20 ml), stirring speed 1500 rpm; [b] 220 mg catalyst; [c] 217 mg catalyst; [d] 450 mg catalyst.

Under comparable conditions, Pd/C and Pt/C had lower selectivities due to the significant formation of undesired $C_2$ and $C_1$ products. Hutchings *et al.* further argued that by an increased amount of catalyst and abundant supply of $O_2$, tartronic acid will be formed in significant amounts due to consecutive oxidation of glyceric acid. This is also observed when decreasing the concentration of glycerol and base. The role of the base was proposed to initiate dehydrogenation via H-abstraction of one of the primary OH groups of glycerol. This overcomes the rate limiting step in the oxidation process.

Hutchings' group also studied Pd and Pt catalysts, both showing high selectivities to glyceric acid. However, without the use of a base, the main products were the non-desired $C_1$ by-products, e.g. $CO_2$, HCHO. After adding base, the formation of $C_1$ by-products was eliminated for Pt [45].
It can be concluded that the use of a base is necessary to avoid non-desired $C_1$ by-products and overcome the rate limiting step in the oxidation process.

P. Claus *et al.* and F. Porta *et al.* performed studies on the influence of the reaction conditions (temperature, catalyst amount, preparation method, NaOH/glycerol ratio & $O_2$ pressure) for the selective oxidation of glycerol using Au as catalyst [46-48]. The catalyst preparation method has been studied and optimized to the goldsol method [47]. The oxygen pressure does nearly not influence the reaction rates of the glycerol oxidation. The initial reaction rate increases strongly by increasing the base concentration until a NaOH/glycerol molar ratio of 2 and above. The initial reaction rate is also dependent on the catalyst amount with the mass transfer limited regime occurring below a glycerol/Au ratio of 2500 [46]. With higher temperatures a higher reaction rate constant $k$ is measured [46] but also a decrease in selectivity [48].

### 1.4.6 Bimetallic catalyst

Hutchings *et al.* examined the idea of using bimetallic supported catalysts in the liquid phase oxidation of glycerol. Alloying Pd with Au was observed to significantly enhance the selective oxidation of glycerol. The most active catalysts were formed using a sol immobilization preparation method [49]. This method leads to unsupported homogeneous alloys being formed with narrow particle size distributions. After preparing these homogeneous alloys, they are being deposited on supports. In contrast,

impregnation of the supports with $HAuCL_4$ and $PdCl_2$ leads to larger particle sizes with Pd enriched surfaces. Finally, to observe high activity coupled with good selectivity to glycerate (the desired product), the surface composition of the nanoparticles requires a significant (1 wt.% Au) contribution from Au [45].

Prati *et al.* also investigated the liquid phase oxidation of glycerol promoted by bimetallic Pd-Au catalysts supported on graphite prepared by a sol immobilization synthesis [4]. A significant improvement in the activity of the bimetallic system was observed with respect to monometallic systems. Also, the selectivity to glyceric acid was found to be dependent on the reaction temperature and catalyst preparation methods (reducing agent, stabilizing agent, particle size, support type) [4, 50-56].

Liu *et al.* reported the efficient conversion from glycerol to lactic acid by aerobic oxidation under mild conditions (363 K, 1 atm $O_2$, $2.5x10^{-3}$ mmol metal, 0.22 $molL^{-1}$ glycerol in $H_2O$, NaOH/glycerol = 4:1), using a Au-Pt/$TiO_2$ catalyst. Combination of Au and Pt (Au/Pt = 1:1) on $TiO_2$ led to an activity of 517.1 $h^{-1}$ with a lactic acid selectivity at 85.6%. This high selectivity to lactic acid was measured even at 100% glycerol conversion, corresponding to approximately an 86% yield of lactic acid [23].

Pagliaro *et al.* reported one-pot oxidation of glycerol to ketomalonic acid by using iron based homogeneous and heterogeneous catalysts [57].

Waymouth *et al.* and Varma *et al.* both reported the efficient conversion of glycerol to dihydroxyacetone by using Pd and Pt-Bi/C catalysts respectively. Waymouth *et al.* reported the catalytic oxidation of glycerol with 5 mol% palladium (2.5 mol%) at room temperature leading to a 97% conversion in 24 hours and >96% selectivity to dihydroxyacetone [58]. Varma *et al.* measured a maximum dihydroxyacetone yield of 48% at 80% glycerol conversion under optimised conditions (80 °C, 30 psig $O_2$ pressure, pH=2 ), using a 3 wt % Pt, 0.6 wt % Bi catalyst supported on AC [59].

### 1.4.7 Proposed reaction mechanisms

The big challenge associated with these catalytic reactions is to control and direct the reaction pathway to the desired products. Even though various studies on the catalytic performance in the reaction of glycerol oxidation have been performed, there is no general consensus about the pathway. Difference in basic and acidic media, choice of the metal and different gold particle sizes significantly affect the catalytic performance and therefore the direction of the reaction pathway.

Hutchings *et al.* proposed the following reaction mechanism shown below (Figure 6). According to this pathway, glycerol can undergo two different routes of oxidation. By oxidizing either one primary or one secondary OH group, glyceraldehydes and dihydroxyacetone are formed respectively. Glyceric acid, tartronic acid and oxalic acid are all detected in significant quantities with glyceric acid dominating. These are the sequential oxidizing products from the glyceraldehyde route.
However, dihydroxyacetone with its oxidized products are not reported.
Remarkably, in Hutchings' experiments, glyceraldehyde was always observed in a relatively large quantity, which was hardly observed by other groups [45]. This can be due to the experimental conditions used.

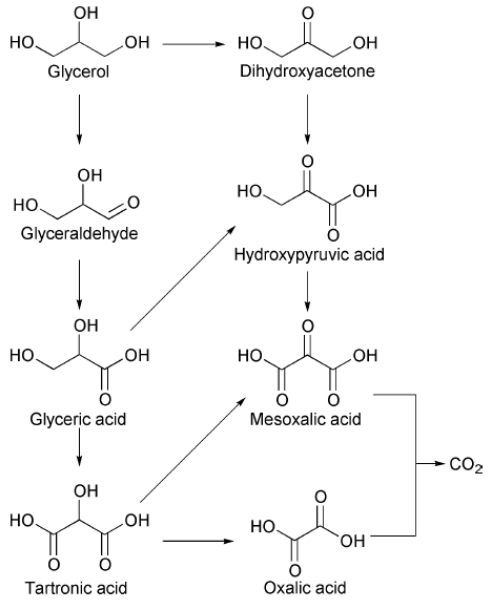


***Figure 6: Proposed mechanism by Hutchings' group [2]***

Prati *et al.* proposed the reaction mechanism from a different perspective (Figure 7). Under basic conditions dihydroxyacetone and glyceraldehyde can interconvert. Plus, the oxidation of the aldehyde group is faster than the oxidation of the OH group. This could enhance the overall selectivity to glyceric acid with respect to the first step of selectivity (intrinsic selectivity of the catalyst). It is further argued that the overall selectivity of the reaction is derived from the combination of two factors; the nature of the catalyst (which determines the starting amounts of hydroxyacetone and glyceraldehyde) and the experimental conditions (NaOH/glycerol ratio, glycerol concentration, temperature, & glycerol/catalyst ratio). High overall selectivity can be achieved by using either a catalyst that is highly selective to glyceraldehyde, or by using a less selective catalyst under basic conditions that favours dihydroxyacetone and glyceraldehyde interconversion. In the former case, the rapid oxidation of the glyceraldehyde (kinetic control) favours the production of glyceric acid instead of the production of dihydroxypyruvic acid [48].

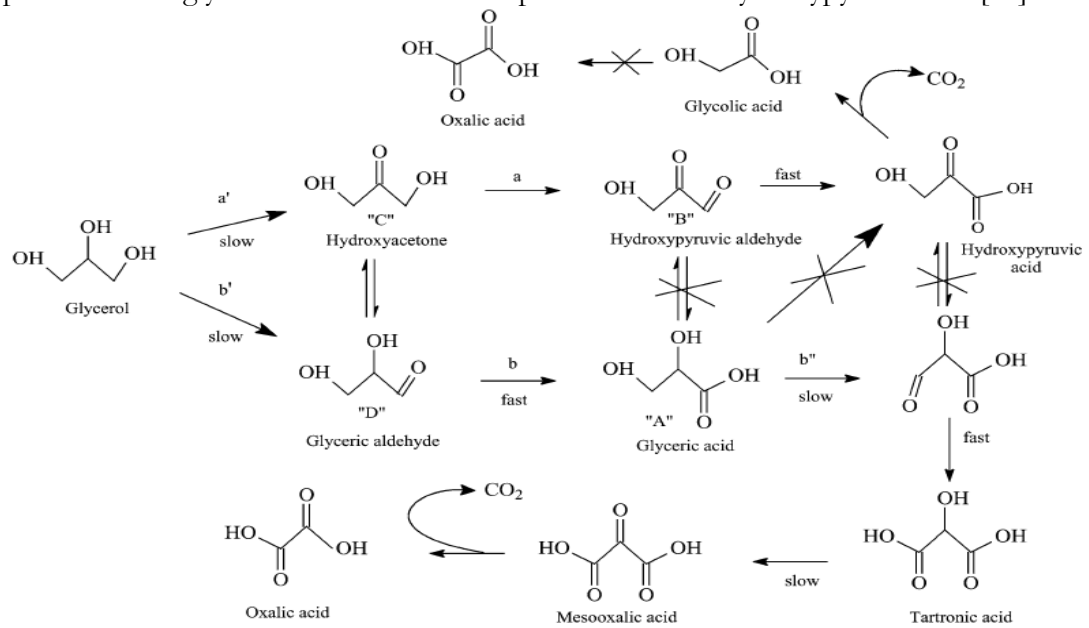


***Figure 7: Proposed mechanism by Prati's group [53]***

David *et al.* proposed a reaction mechanism shown in the figure below (Figure 8). The $H_2O_2$ formation during the reaction was examined with Pd, Au and Pd-Au catalysts. It was found that $H_2O_2$ contributed to the observed C-C cleavage, thus detrimental to the selectivity towards glyceric acid. However, palladium was proposed to catalyze the decomposition of the side product $H_2O_2$ which was formed on the surface of both palladium and gold. There was no significant rate enhancement for the bimetallic catalysts compared with monometallic catalysts. Besides, hydroxyl was found to enhance the formation of $H_2O_2$, leading to higher activity but lower selectivity with high OH- concentrations [41, 60-61].

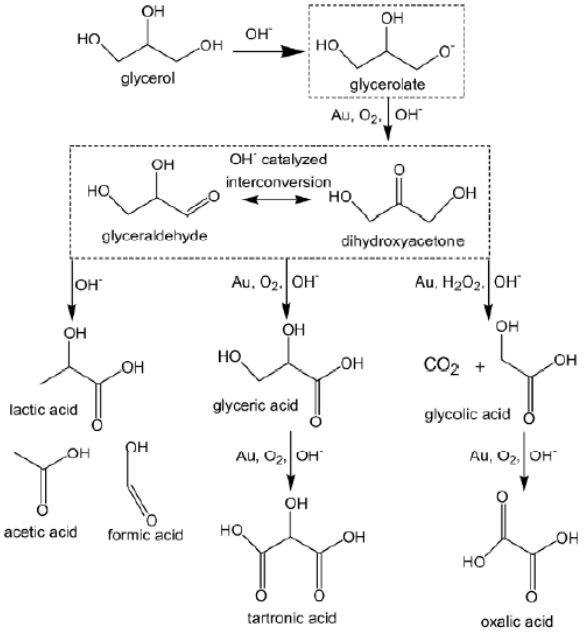


***Figure 8: Proposed mechanism by Davis' group [416041]***

## *1.5 Pd/Au catalysis in the Wong lab*

Pd on Au catalysts have been widely studied in the application of groundwater remediation by Wong *et al.* [6-11].

### 1.5.1 Catalyst promoted hydrodechlorination of trichloroethene

Trichloroethylene (TCE), a man-made chlorinated hydrocarbon, is suspected to have a carcinogenic nature. Therefore remediation of TCE contaminated soils and groundwater is an issue. Groundwater remediation through the catalytic breakdown of the undesired contaminants is a more effective and desirable approach than the conventional physical displacement methods of air-stripping and carbon adsorption. The catalysis and nanomaterials group (the Wong lab) at Rice University conducted research on the HDC (hydrodechlorination) of TCE using a Pd-on-Au catalyst, to improve the potential of this catalyst as a groundwater remediation technology.

The first version of Pd/Au nanoparticles were synthesized with a 20 nm Au core by the Turkevich–Frens (citrate reduction) method, and Pd metal was deposited using Pd chloride salt ($PdCl_2$) and ascorbic acid as reducing agent. The colloidal catalyst had extremely high reaction rate constants for the HDC of TCE, with the most active composition exhibiting a first-order rate constant that was >10, >70 and >2000 than

monometallic Pd nanoparticles, $Pd/Al_2O_3$ and Pd black. The second version Pd/Au nanoparticles were designed as a ~4 nm Au core using citrate-tannic acid reduction with various Pd surface coverages by hydrogen reduction. Which is a more robust metal reduction step than using ascorbic acid, with the latter occasionally leading to colloidally unstable nanoparticle suspensions. The smaller nanoparticles were catalytically more active, with the most active composition (~13 wt% Pd) twice as active as the 20 nm nanoparticles with 1.9 wt% Pd [7].
Both 20 nm and ~4 nm Pd/Au nanoparticle catalysts showed a volcano-shaped[2] reactivity dependence on Pd surface coverage (Figure 9). The rate of HDC was highest with ~4 nm Pd/Au nanoparticles at 60-70% Pd coverage [5].
The promotion effect of Au on Pd was ascribed to three possible factors; a geometric effect (formation of 2D or 3D Pd clusters or ensembles on the Au surface), a mixed metal site effect (formation of Pd-Au surface species as a new population of active sites), an electronic effect (electron interaction between Pd and Au atoms) [7, 9].

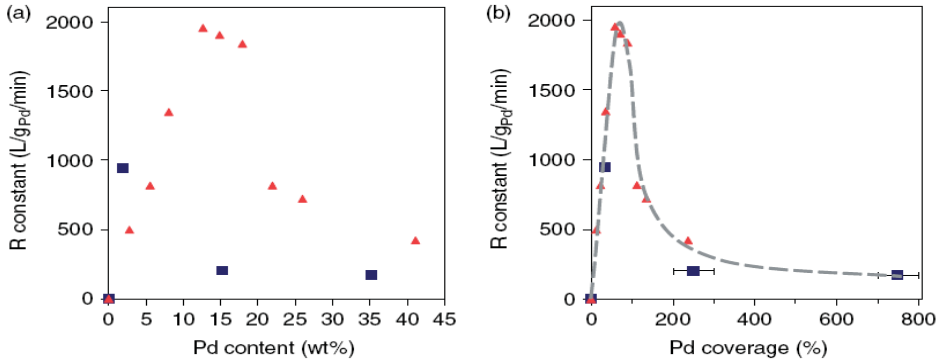


***Figure 9: Pseudo-first-order reaction constants for Pd/Au nanoparticles with 20 nm (blue squares) and ~4 nm (red triangles) Au core, plotted as a function of (a) Pd weight content and (b) Pd surface coverage [5, 6****Error! Reference source not found.****]***

### 1.5.2 Catalyst promoted hydrodechlorination of tetrachloroethylene

Tetrachloroethylene (also known as perchloroethylene or PCE) is one of the most pervasive environmental contaminants. It is a known central nervous system depressant and is listed as a probable carcinogen compound in humans [63].
The Wong lab extended catalytic work to test the Pd/Au nanoparticles for the HDC of PCE.

Catalytic testing of the Pd/Au nanoparticles was performed with a range of surface coverages together with Pd nanoparticles and supported Pd catalysts ($Pd/Al_2O_3$ and Pd/resin). It was demonstrated that the Pd/Au nanoparticles can catalyze the HDC reaction of PCE. The catalysts activity shows a volcano-shaped pattern when plotted against the Pd surface coverage (Figure 10). The ~4 nm Pd/Au nanoparticles proved to be much more active than the Pd based materials, with the most active (~80% Pd coverage) at least one order of magnitude more active. Au alone is inert in the HDC of PCE. However, it is suggested that the enhancement of the underlying gold is of geometric and electronic effects. Furthermore, the Pd coverage (~80%) at which HDC of PCE is the most active is slightly larger than that in HDC of TCE (~67%). This might be due to the fact that the PCE molecule is larger than that of TCE, which requires more

[2] The volcano-shaped curve is one of the most fundamental concepts in heterogeneous catalysis. It is obtained when the activity of the catalysts for a certain reaction is plotted as a function of a parameter relating to the ability of the catalyst surface to form chemical bonds to reactants, reaction intermediates, or products [6262].

active sites to bind.

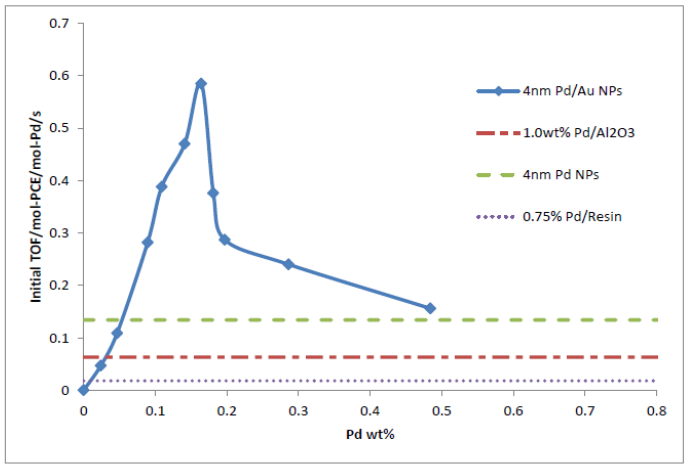


***Figure 10: Volcano-shaped plot of the HDC reaction for PCE with various Pd weight percentages of Pd-on-Au nanoparticles***

### 1.5.3 Indirect evidence of Pd/Au nanostructure

To fully understand which effect is dominant as a way to correlate nanostructure with observed promotion effect, several tools have been employed to track the evidences, such as TEM (Transmission Electron Microscopy), XPS (X-ray Photoelectron Spectroscopy) and EXAFS (Extended X-ray Absorption Fine Structure) [5, 7].

TEM provides particle size analysis from individual particles. The nanoparticle samples were imaged by analysis of imaging with a JEOL 2010 transmission electron microscope. The TEM images show that the mean particle sizes for the monometallic Au, monometallic Pd and 0.6ML Pd/Au nanoparticles were similar at ~4 nm (Figure 11). However, TEM was unable to capture the existence of the Pd layer visually as Pd is in the order of one atom thick.

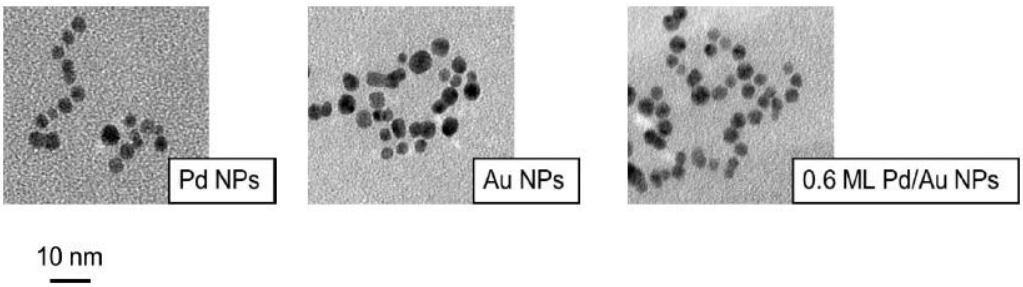


***Figure 11: TEM images of Pd, Au & Pd/Au nanoparticles (Courtesy of Dr. Y.L. Fang)***

XPS was performed to show a systematic change in Pd d-orbital binding energy states with different surface coverages (Figure 12). This indicates that the electronic structure of the Pd metal was modified by the Au, which would result only if the Pd metal were in close contact with the Au nanoparticles [6].

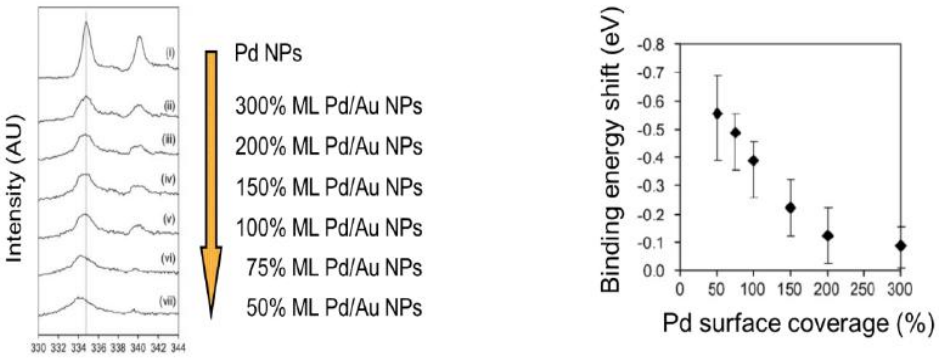


***Figure 12: Pd binding energy shifts as a function of Pd surface coverage [6****Error! Reference source not found.****]***

### 1.5.4 Direct evidence of Pd/Au nanostructure

EXAFS is a powerful tool to determine information on the local structure of bimetallic catalysts. This detection method is extensively described in Chapter 3.4.

In the work done by Fang *et al.* [5**Error! Reference source not found.**] Pd/Au nanoparticles were confirmed to have a core-shell structure with EXAFS data (Figure 13). The Pd atoms were located on the surface of a Au-rich core. Moreover, Pd/Au nanoparticles nearly had all its Pd nanoparticles as surface atoms of which only ~20% were oxidized, while monometallic Pd nanoparticles had 25-35% of its Pd atoms at the surface from which nearly all were oxidized. In the HDC of TCE, mild reaction conditions were used (room temperature, atmospheric pressure), under which the oxidized surface of the monometallic Pd nanoparticles was not reduced. Thus, the metallic Pd atoms of the Pd/Au nanoparticles are suggested to behave as active sites for aqueous phase HDC of TCE at room temperature. Au nanoparticles appear to have a unique ability to stabilize surface Pd atoms in metallic form, possibly leading to a set of high active sites. This is not present in monometallic Pd nanoparticles under ambient temperature reaction conditions.

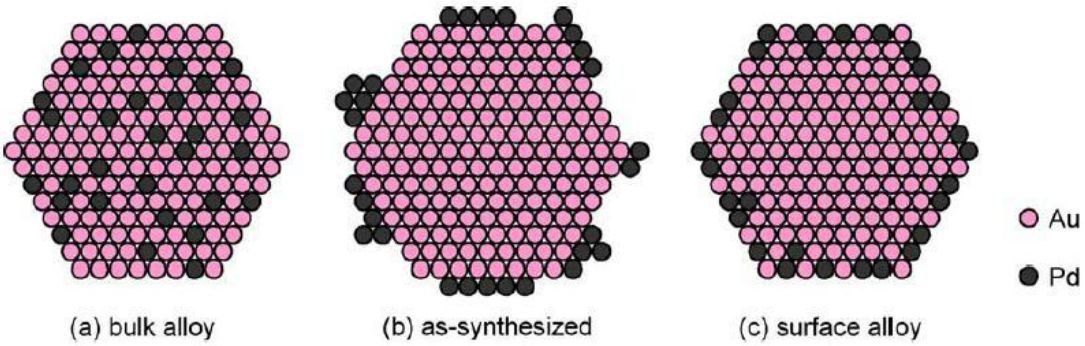


***Figure 13: Idealized cross-sections of (a) a Pd/Au alloyed nanoparticle and core-shell nanostructures of a Pd/Au nanoparticle (b) in the as-synthesized form and (c) after reduction in $H_2$ at 300 °C [11]***

# 2 Part I - Modulating supported palladium-on-gold catalysts for glycerol oxidation with varying palladium surface coverages

The liquid-phase selective oxidation of glycerol has been extensively studied using mainly supported noble metal nanoparticles, such as Pt, Pd and Au [3, 24-27].
Hutchings *et al.* observed an enhanced selectivity by alloying Pd with Au as supported catalyst [49]. Prati *et al.* showed a significant improvement in the activity of bimetallic Pd-Au catalyst on support in the liquid phase oxidation of glycerol with respect to the monometallic systems [4]. In other studies, Villa *et al.* observed a strong synergistic effect present in a large range of Au/Pd on AC at atomic ratio in the liquid phase oxidation for glycerol [54].
However, systematic investigation of catalytic activity with alternate Pd surface coverages on support in the selective oxidation of glycerol has not yet been reported.

In this work, a series of AC supported ~4 nm Pd/Au catalysts with different Pd surface coverages ranging from 10-80% were prepared. The catalytic properties in the liquid phase oxidation of glycerol in water using oxygen as the oxidant are reported. Monometallic gold and palladium catalysts on AC support have been tested equally, to investigate the effect of the support material and the nature of the active sites.
The catalytic activity with various Pd surface coverages was characterized by HPLC and is reported in terms of TOFs (turnover frequency).

## *2.1 Hypothesis*

The following hypothesis is proposed, for Pd/Au bimetallic catalysts with respect to their enhanced activity and selectivity in liquid phase oxidation of glycerol:

- The activity and selectivity of Pd/Au bimetallic catalysts in the selective oxidation of glycerol can be regulated by Pd surface coverage as a way to maximize the yield to glyceric acid.
- The Pd surface coverage has a volcano-shaped optimum with respect to activity and selectivity.

Thus, there might be a Pd/Au nanoparticle with specific Pd surface coverage that can maximize the yield (activity x selectivity) of the desired compound.

## *2.2 Catalyst preparation*

Au nanoparticles from ~4 nm can be synthesized through a sodium citrate-tannic acid reduction method. The amounts of Pd to be deposited can be determined by the magic cluster model[3] for various Pd surface coverages.

### 2.2.1 Preparation of ~4 nm Au nanoparticles

Gold nanoparticles were synthesized according to Nutt *et al.* [9] by modifying the method reported by Geuze *et al.* [64]. ~4 nm Au nanoparticles were synthesized via a sodium citrate-tannic acid reduction method. Several salt solutions were prepared prior to the

[3] Further discussed in Chapter 2.2.6

reducing. A gold salt solution was prepared by diluting 0.20 mL of a 5 wt% $HAuCl_4$ solution (0.126 M; 5 g of $AuCl_3$•$3H_2O$ (99.99%, Sigma–Aldrich) in 95 mL $H_2O$) in 79.8 mL of Nanopure water (>18 MΩ-cm, Barnstead NANOpure Diamond). Three stock solutions were prepared; 1 wt% trisodium citrate solution (Cit sol), 1 wt% tannic acid solution (TA sol) and 25 mM potassium carbonate solution ($K_2CO_3$ sol). These were prepared by separately dissolving 0.2 g of trisodium citrate dihydrate (>99.5%, Fisher), 0.2 g of tannic acid (>99.5%, Sigma–Aldrich) and 0.069 g potassium carbonate (>99.5%, Sigma–Aldrich) into 20 ml of Nanopure water. The reducing mixture was prepared by adding 5 ml of TA sol, 5 ml of $K_2CO_3$ sol and 4 ml of Cit sol into 6 mL of Nanopure water and was heated to 60 °C.
Once this temperature was reached, the tannic acid solution was added to the gold chloride solution. The formation of gold nanoparticles was apparent by the immediate colour change from pale yellow to reddish-brown, indicative of gold nanoparticles. The mixed solution was then heated to boil for 2 minutes and removed from the heat source. A portion of the water volume (~20%) evaporated during the boiling step. Therefore, an appropriate amount of DI water was added to adjust the sol volume to 100 ml. The final fluid had a dark brown-red colour and was left to age overnight (at room temperature) before being stored in a refrigerator. Au nanoparticles in the final fluid were about 4 nm in diameter according to TEM and the concentration was calculated to be $1.07x10^{14}$ nanoparticle/mL assuming 100% reduction of Au salts.

### 2.2.2 Preparation of bimetallic Pd/Au nanoparticles

Bimetallic Pd/Au nanoparticles were prepared by reducing Pd precursor in the preformed Au nanoparticles sol with hydrogen. Specified volumes of 2.49 mM $H_2PdCl_4$, which was prepared by dissolving 0.0422 g $PdCl_2$ (99.99%, Sigma-Aldrich) in 95 ml Nanopure water with 500 µl $HCl_{(aq)}$ (1 M, Fisher Scientific), were added to 200 mL stock Au nanoparticle sol. Utilizing the magic cluster model, the amount of palladium solution needed to add for various surface coverages on the Au nanoparticles is calculated [8, 9]. For example, 5.43 mL of the Pd solution was added drop wise to 101 mL of Au nanoparticles sol corresponding to a surface coverage of 60%. The mixture was then vortexed vigorously for 5 minutes followed by bubbling with $H_2$ gas (99.99%, Matheson) through the solution for 30 minutes to fully reduce the palladium onto the surface of the Au nanoparticles.

### 2.2.3 Preparation of ~4 nm Pd nanoparticles

Palladium nanoparticles were prepared using the same procedure for Au nanoparticle synthesis, except that the Au salt solution was replaced by 10.4 mL of a $H_2PdCl_4$ solution (2.49 mM; PdCl2, 99.99%, Sigma–Aldrich) combined with 69.6 mL of $H_2O$. The boiling time was also increased to 25 min. The resulting yellow fluid was aged overnight at room temperature. After this DI water was added to a total volume of 200 mL, a coffee-brown coloured fluid remained. This sol contains ~4 nm Pd nanoparticles and has a calculated particle concentration of $2.9x10^{15}$ nanoparticle/L.

### 2.2.4 Preparation of activated carbon supported Au, Pd, Pd/Au catalysts

To prepare 1.0 wt% gold on active carbon catalyst (1 wt% Au/AC), 1 g of AC (Vulcan XC-72, Cabot) was added into 202 mL of ~4 nm Au sol (49.25 mg Au/L), and stirred vigorously for 12 hrs. After which it was centrifuged at 14000 rpm under 4 °C for 40 min. The carbon slurry was collected and dried overnight in a vacuum oven at 60 °C to

fully remove moisture. The catalyst was then crushed into powder for storage and catalytic testing.

0.32 wt. % palladium on AC catalyst (0.32 wt. % Pd/AC) was prepared in the same manner by mixing 200 ml of ~4 nm Pd nanoparticle sol (15.90 mg Pd/L) with 1 g of AC.

Pd/Au supported on AC catalysts were also prepared in the same procedure by mixing 202 ml of ~4 nm Pd/Au nanoparticle sol of a specific Pd surface coverage with 1 g of AC. Pure AC underwent all the same operations as a control.

### 2.2.5 Sodium citrate-tannic acid reduction method

The ~4 nm Au nanoparticles used were synthesized through a sodium citrate-tannic acid method reported by Geuze *et al.* [64].

The colloidal Au sols get formed in three steps:

1 Reduction of $Au^{3+}$ by tannic acid occurs due to oxidation of hydroxyl groups to carbonyl groups to form quinines
$AuCl_4^- + 3R\text{-}OH \rightarrow Au^0 + 3R{=}O + 3H^+ + 4Cl^-$
2 Nucleation; Au atoms cluster and form seeds/nuclei from which Au nanoparticles arise [65]
3 Particle growth due to condensation of Au on the nuclei surface [66]

Trisodium citrate and tannic acid both serve as reducing agents, meanwhile polymers formed from tannic acid during and after the reduction serve as stabilizer. The size of the Au nanoparticles is inversely related to the tannic acid concentration. Thus, by changing the concentration of tannic acid, Au particles with sizes ranging from ~3 to ~12 nm can be synthesized (Figure 14). The more tannic acid used, the smaller the size of the particle. This method has several advantages:

- Well established method (since 1985)
- Easy to use (no special equipment needed, fast process)
- Good reproducibility
- Good monodispersity (standard deviation in size distribution less than 35%)
- Uses same stabilizing agents for all sizes
- Used on other research performed in the group (HDC of TCE & PCE) which makes it better to compare results

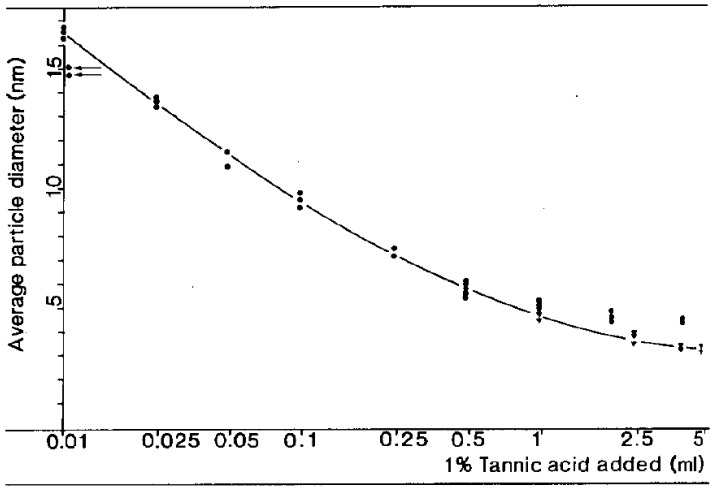


***Figure 14: The influence of tannic acid concentration during gold sol formation on the size of the gold particles [64]***

### 2.2.6 Magic cluster model

In the synthesis of Pd/Au nanoparticles with various surface coverages, the nanoparticles were modelled as gold "magic clusters" with a Pd shell of variable coverages to relate the Pd loading to a core/shell bimetallic structure[4]. In the magic cluster model (Table 3)[9, 67-69], a nanoparticle is treated as a central atom surrounded by closed shells of identical atoms. This provides a helpful calculation method for estimating the Au nanoparticle concentration and the Pd surface coverage. ~4 nm Au nanoparticles were approximated as containing 7 shells of Au atoms based on the assumption of complete reduction of the Au precursor to form Au nanoparticles, with an estimated concentration of $1.07 \times 10^{14}$ nanoparticle/mL. Pd has an atomic radius of 1.40 Å [70]. Therefore, the reductive deposition of Pd atoms onto the Au nanoparticle surface was considered to be equivalent to the formation of an eighth shell of metal atoms (Figure 15).

***Table 3: Magic cluster calculation of Au nanoparticles [9]***

| Shell number ($n$) | Number of atoms in shell ($n_{atom}$)[a] | Total number of Au in NP($n_{tot}$)[b] | Calculated Au NP diameter (nm) |
|---|---|---|---|
| | 1 | 1 | 0.27 |
| 1 | 12 | 13 | 0.80 |
| 2 | 42 | 55 | 1.34 |
| 3 | 92 | 147 | 1.88 |
| 4 | 162 | 309 | 2.41 |
| 5 | 252 | 561 | 2.95 |
| 6 | 362 | 923 | 3.48 |
| 7 | 492 | 1415 | 4.02 |
| 8 | 642 | – | – |
| 9 | 812 | – | – |

[a] Equation: $n_{atom} = 10n^2 + 2$.
[b] Equation: $n_{tot} = (10n^3 + 15n^2 + 11n + 3)/3$.

Thus, a ~4 nm Au nanoparticle with a complete shell of Pd atoms, or 100% coverage, is readily calculated to have a Pd content of 19.7 wt%. Surface coverages above 100% refer to the formation of additional shell on top of the complete eight Pd shell. For example, 150% Pd coverage means 100% coverage of the 8th shell plus 50% coverage of the 9th

[4] In the work done by Fang *et al.* Pd/Au nanoparticles were confirmed to have a core-shell structure with EXAFS data [5]

shell, while 300% Pd coverage refers to a complete coverage of Pd on the 8th, 9th and 10th shells.

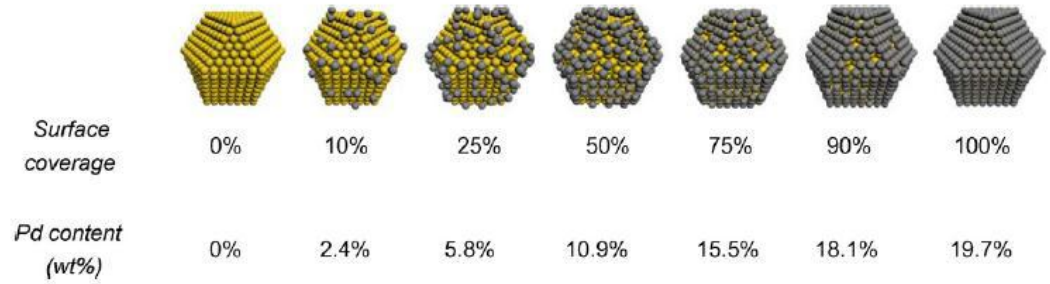


***Figure 15: Schematic of Pd/Au nanoparticles idealized as magic clusters, with a 4-nm Au core and variable Pd surface coverage from 0 to 100% [6]***

With the information of shell atom number, we are able to calculate how much $Pd^{2+}$ precursor is needed to form a specific surface coverage on the ~4 nm Au nanoparticles. Below is a table showing the results of total Pd weight percentage, total Pd molar percentage and amount of $PdCl_4$ needed (Table 4).

***Table 4: Calculation for 4 nm Au with various Pd surface coverages***

| Pd surface coverage | Total Pd wt% | Total Pd mole % | mL of $PdCl_4$ added |
|---|---|---|---|
| 0% | 0.0 | 0.0 | 0.00 |
| 10% | 2.4 | 4.3 | 0.45 |
| 20% | 4.7 | 8.3 | 0.91 |
| 30% | 6.8 | 12.0 | 1.36 |
| 40% | 8.9 | 15.4 | 1.81 |
| 50% | 10.9 | 18.5 | 2.26 |
| 60% | 12.8 | 21.4 | 2.72 |
| 70% | 14.6 | 24.1 | 3.17 |
| 80% | 16.4 | 26.6 | 3.62 |
| 90% | 18.1 | 29.0 | 4.08 |
| 100% | 19.7 | 31.2 | 4.53 |
| 110% | 21.2 | 33.8 | 5.10 |
| 150% | 26.9 | 42.5 | 7.39 |
| 300% | 42.4 | 63.4 | 17.33 |

## *2.3 Catalytic test - glycerol oxidation semi-batch reaction*

The aqueous-phase oxidation of glycerol (ACS reagent, ≥99.5% from Sigma-Aldrich) was performed in a screw-cap bottle (250 mL, Alltech), which was wrapped with Teflon tape threads and sealed with a Teflon-rubber septum. To avoid pressure build-up, a single syringe was pierced through the Teflon-rubber septum as a pressure/$O_2$ relief device.

A magnetic stirrer, Nanopure water (101 mL), 2 mL of 10 M NaOH (prepared by dissolving 40 g NaOH (≥99.5%, Sigma-Aldrich) in 100 mL DI water) and 0.2 g of catalyst were added to the reactor. The reactor was then kept at 60 °C in a water bath and bubbled with $O_2$ gas (99.99%, Matheson) for 15 min while stirring to saturate with oxygen. After this, 2 mL of 5 M glycerol (prepared by dissolving 46.047 g glycerol (ACS reagent, ≥99.5%, Sigma-Aldrich) in 100 mL DI water) was added to the reactor by

insertion with a syringe. The stirring rate was maintained at ~1000 rpm[5] while $O_2$ was continually fed at 0.12 L/min controlled by a mechanical flow meter. The mixture was stirred for 1 minute for homogeneity before taking the first sample. Samples were periodically removed via a sample tube, which was removed, washed and dried after every sample. Table 5 shows the used experimental conditions for the selective oxidation of glycerol reaction.

***Table 5: The experimental conditions in the selective oxidation of glycerol reaction***

| | |
|---|---|
| Glycerol (5 mol/L) | 2 mL |
| NaOH (10 mol/L) | 4 mL |
| NaOH/glycerol molar ratio | 4:1 |
| DI water | 101 mL |
| Catalyst | 0.2 g |
| Glycerol/Au atom molar ratio | 1083 |
| Temperature | 60 °C |
| O2 flow rate | 0.12 L/min |
| Stirring rate | ~1000 rpm |
| Total volume | 107 mL |

## *2.4 Method of analyzes*

The samples from the reaction (500 µL) are black turbid liquid, when filtered (3.1 µm microfiber) a transparent light yellow or clear liquid remains. These samples are analyzed by an ion-exclusion high-performance liquid chromatograph (HPLC).

### 2.4.1 High-performance liquid chromatography (HPLC)

The composition of the liquid samples was determined using a Shimadzu Prominence SIL 20 system (Shimadzu Scientific Instruments, Inc., Columbia, MD) equipped with an HPX-87H organic acid column (Bio-Rad, Hercules, CA) and an UV detector. The mobile phase consisted of aqueous sulphuric acid (30 mM) which was set at a flow rate of 0.6 $cm^3$ $min^{-1}$. The column was operated at 315 K. The analysis for one sample was completed in 30 min. The concentrations of each compound in the product mixture were determined using calibration curves obtained by analysing standard solutions of known concentrations (Table 6). The calibration curves were re-obtained every month to avoid any changes in retention times and peak areas.

***Table 6: Average retention time and standard curve for each compound in the selective oxidation of glycerol***

| Compound | Retention time/min | Standard Curve/mM |
|---|---|---|
| Glycerol | 26.86 | Peak area/75346.64 |
| Glyceric acid | 22.06 | Peak area/143029 |
| Oxalic acid | 17.72 | Peak area/74411 |
| Glycolic acid | 25.95 | Peak area/49381 |
| Tartronic acid | 17.63 | Peak area/96952 |
| Formic acid | 28.41 | Peak area/15921.78 |
| Acetic acid | 30.80 | Peak area/28152.76 |
| Lactic acid | 25.78 | Peak area/63869.06 |

[5] See Appendix B

## 2.5 Results and discussion

Reaction rate constants were calculated by assuming first-order dependence on glycerol concentration. The pseudo first-order reaction kinetic was validated by the concentration profiles for all the catalysts in this study (Figure 16).

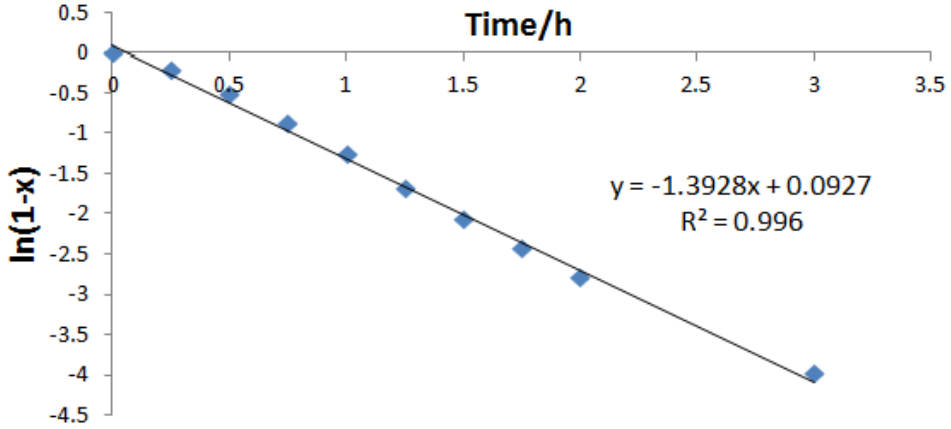


***Figure 16: Pseudo 1st order reaction kinetic for a 60% Pd-on-Au catalyst in the oxidation of glycerol***

The observed reaction rate constant $k_{obs}$ ($hr^{-1}$) is defined as:

$$\frac{-dC_{gly}}{dt} = k_{obs} \times C_{gly}$$

The catalytic rate constant $k_{cat}$ ($L/g_{metal}/h$) is defined as $k_{obs}$ normalized by the concentration of total metal ($C_{metal}$) charged into the reactor:

$$k_{cat} = \frac{k_{obs}}{C_{metal}}$$

Initial turnover frequency (mol-glycerol/mol-$Pd_{surf}$/h) is defined as:

$$Initial\ TOF = \frac{{-dC_{gly}(t)}/{dt}_{initial}}{C_{surf(Pd,Au)}} = \frac{k_{obs} \times C_{gly}(0)}{C_{surf(Pd,Au)}}$$

where $C_{surf}^{(Pd,Au)}$ is the total concentration of surface metal.

### 2.5.1 Gold on activated carbon catalyst

The Au/AC catalyst was proven to be active in the oxidation of glycerol as shown in Figure 17(a) and (b) while either AC as purchased or processed was totally inactive.

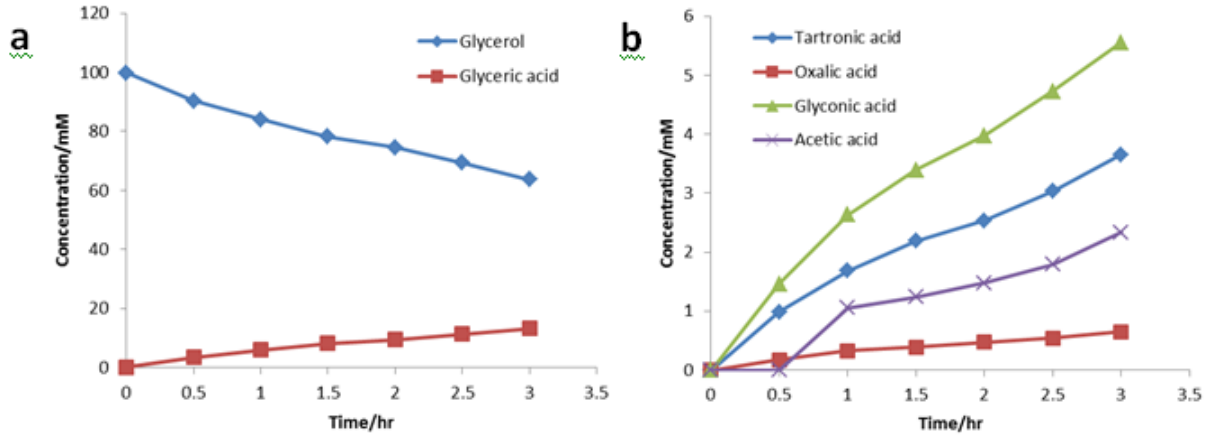


***Figure 17: Concentration profile for 1 wt. % Au/AC catalyst for (a) glycerol and glyceric acid and (b) all the rest products***

Glycerol reached a conversion of 36.1% at a reaction time of 3 h. Glyceric acid was the major product from the full oxidization of one primary OH group of glycerol with a yield of 13.2% at 3 h (selectivity was 42%). While glycolic acid was found to be a secondary major product with a yield of 5.6% (selectivity was 14.3%) due to the cleavage of C-C bonds. Other $C_3$ and $C_2$ compounds, such as tartronic acid, oxalic acid and acetic acid were also found to be present in the mixture, but in very small amounts. The molecule balance by taking all detectable compounds into account was 88.6% at 3 h. The carbon loss was thought to be due to the generation of undesired carbon oxides, neither of which was detected by HPLC.
Appendix C (entry 3) and Appendix D (entry 1) give the calculated activity and selectivity in detail.

### 2.5.2 Palladium-on-gold catalysts: the effect of surface coverage

The reaction was further examined by different types of catalysts as shown in Appendix C. When palladium was added onto the gold surface to form a 10% surface coverage, the activity went up dramatically, leading to a conversion of 58.8% at 3 h. 10% Pd/Au/AC has the same Au loading as Au/AC (1 wt% Au, glycerol: Au = 985). However, the addition of 10% surface Pd (0.025 wt% Pd, glycerol: Pd = 21284) made the calculated TOF for 10% Pd/Au/AC (899 $h^{-1}$) more than double compared with Au/AC (439 $h^{-1}$). When more Pd was deposited onto the Au surface to have higher surface coverages, the activity firstly increased accordingly up to 60% Pd coverage, then dropped off with greater surface coverages. Surface coverages listed over 100% indicate a fully formed layer of palladium atoms covering the gold nanoparticle surface. When the initial TOF was plotted against the Pd surface coverage (Figure 18a), activity was found to be a volcano-shaped function of the surface coverage of the shell Pd atoms on the core Au atoms. The highest activity was observed at a 60% Pd coverage at which 98.1% of the glycerol is converted in just 3 hours time. The reaction profile for 60% Pd/Au/AC is shown in Figure 18. It reached a TOF of 3631 $h^{-1}$, which is nearly 9 times more active than monometallic Au catalyst.

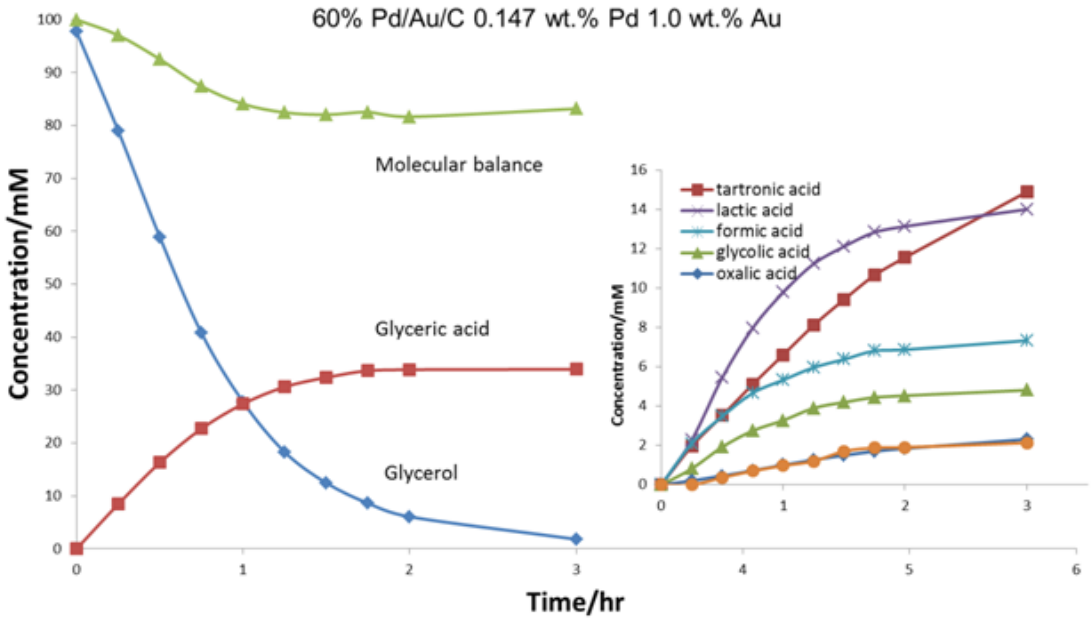


***Figure 18: Concentration profile for 60% Pd/Au/AC catalyst***

The most active catalyst has an almost fully formed layer of palladium atoms with some underlying gold still exposed. This gives implications to the nature of the active sites, which might be Pd-Au interfaces (mixed site effect) or 2-D local surface Pd ensembles (geometric effect) that have a larger population with partial Pd coverages. With a further increase in Pd coverage, the population of Pd-Au interfaces or 2-D Pd ensembles can possibly decease, leading to a decrease in TOF. However, even at surface coverages corresponding to multiple layers (150% Pd/Au/AC), the reaction rates are still significantly higher than monometallic Pd catalysts, suggesting the existence of electronic effects (electron transfer between Pd and Au atoms). The 300% Pd/Au/AC behaved like Pd/AC catalysts in terms of TOF, suggesting all these possible effects were diminished to a great extent. The volcano plots for $k_{cat}$ and $k_{obs}$ (Figure 19b, 24c) also indicate the same trends for all the catalysts.

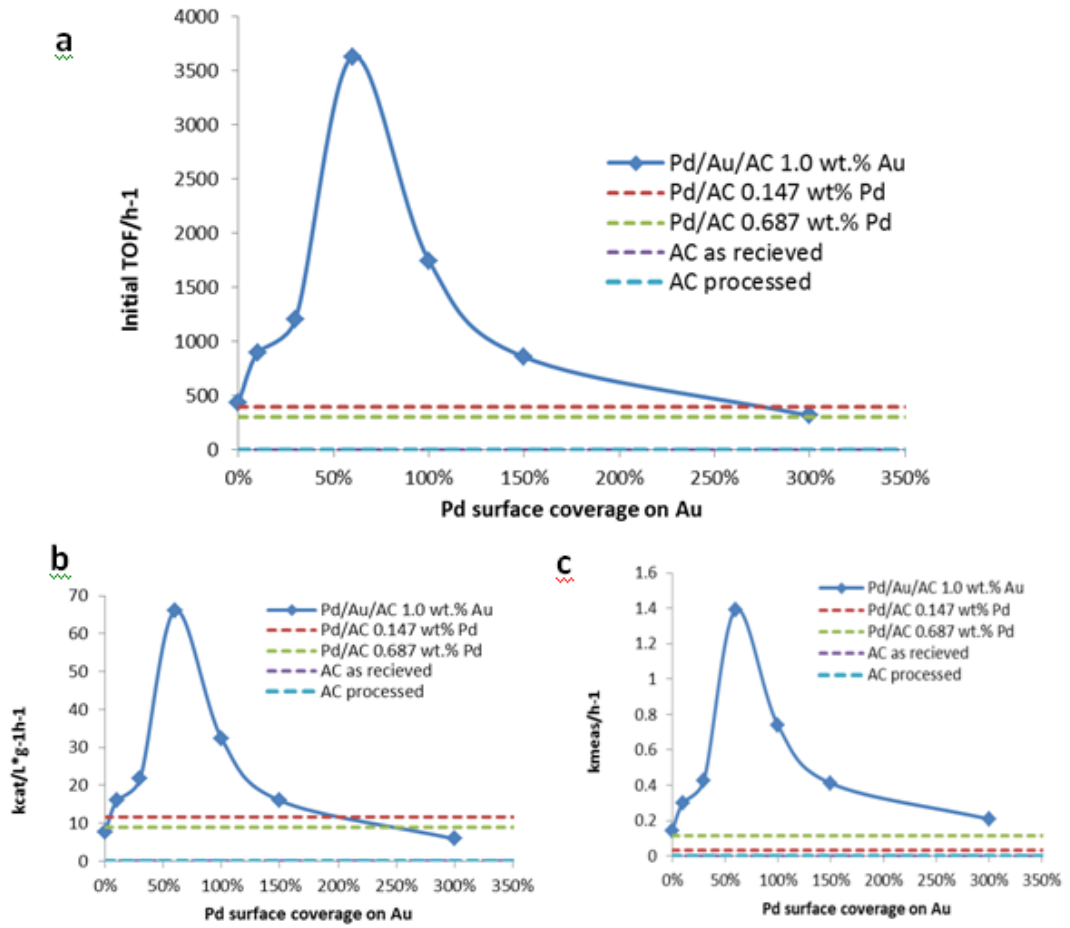


***Figure 19: Reaction rate constants against Pd surface coverage on Au (a) initial TOF (b) $k_{cat}$ (c) $k_{obs}$***

It is noteworthy that Pd catalysts deactivated very fast under experimental conditions, giving initial TOFs of 397 $h^{-1}$ and 304 $h^{-1}$ for 0.147 wt% and 0.687 wt% Pd/AC, equivalent to the TOF value of Au/AC. Several causes of deactivation in selective oxidation of alcohols have been identified by Gallezot *et al.* [39]; irreversible deactivation due to the modification of the catalyst structure (metal sintering or leaching), or reversible deactivation due to poisoning of the metal surface by strongly adsorbed species (oxygen, impurities, products, or by-products). Prati *et al.* further argued that the Pd catalyst deactivation was ascribed to oxygen poisoning proportional to the oxygen partial pressure in the liquid phase oxidation of glycerol [48]. In our case, a pure oxygen flow at 0.12 L/min was used which is over-sufficient for Pd to suffer. Therefore it was thought that an over-oxidation of Pd surface atoms was happening during the oxidation reaction.

### 2.5.3 Selectivity vs. conversion

Selectivity and molecular balance data for all the catalysts is shown in Appendix D.

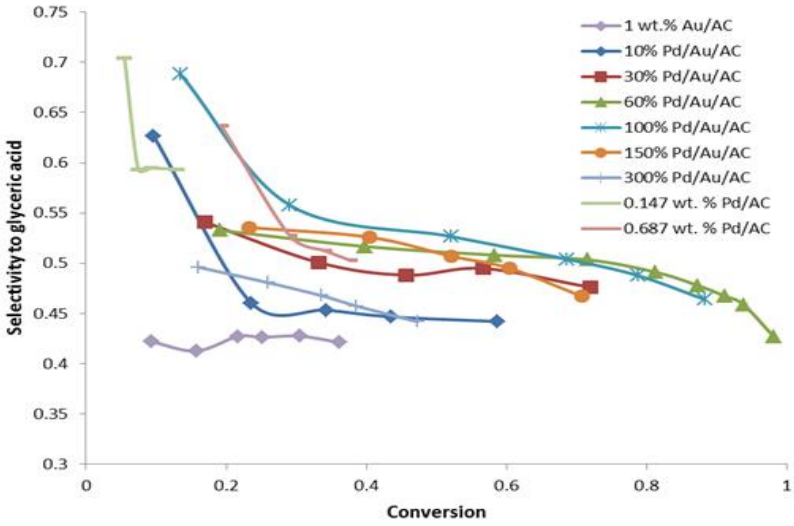


***Figure 20: Selectivity of glyceric acid vs. conversion of glycerol***

When plotting the selectivity of glyceric acid, tartronic acid and lactic acid against the conversion of glycerol for various catalysts (Figure 20, 21 & 22), the following information can be interpreted:

1. Au/AC was less selective than Pd/AC towards glyceric acid. The selectivity for Pd/Au catalysts was higher than Au/AC. The selectivity for Pd/Au has a function with Pd surface coverage, with the highest selectivity detected at ~100%.
2. Selectivity towards glyceric acid dropped during the reaction for Pd/Au catalysts, while increasing towards tartronic acid. At a conversion close to 100%, the decrease in selectivity to glyceric acid (and increase in selectivity to tartronic acid) was dramatic. This result is evidence of the sequential oxidation pathway of glycerol to glyceric acid and further to tartronic acid.

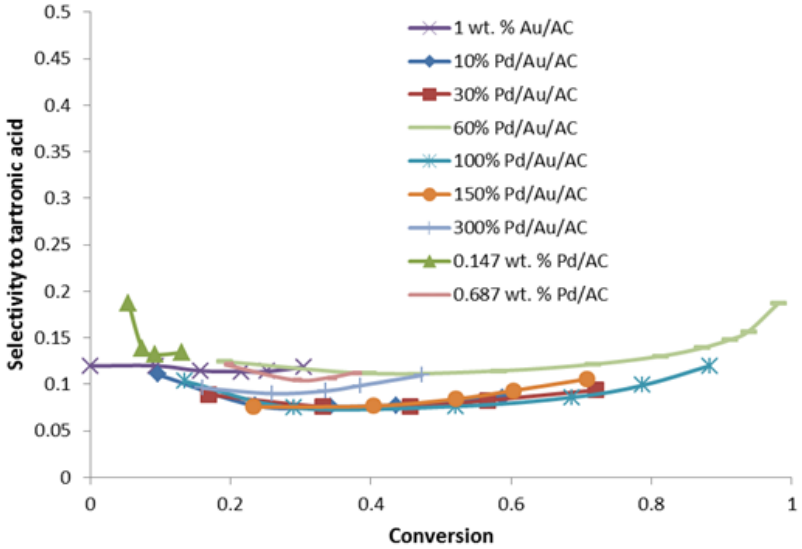


***Figure 21: Selectivity of tartronic acid vs. conversion of glycerol***

When the reaction was close to completion, the concentration of glycerol was consequently low that deep oxidation dominated. More glyceric acid was oxidized into tartronic acid than glycerol into glyceric acid. Furthermore, the decreased selectivity to glyceric acid is greater than the increased selectivity to tartronic acid, indicating that undesired $C_2$, $C_1$ compounds increased in their selectivity as well.

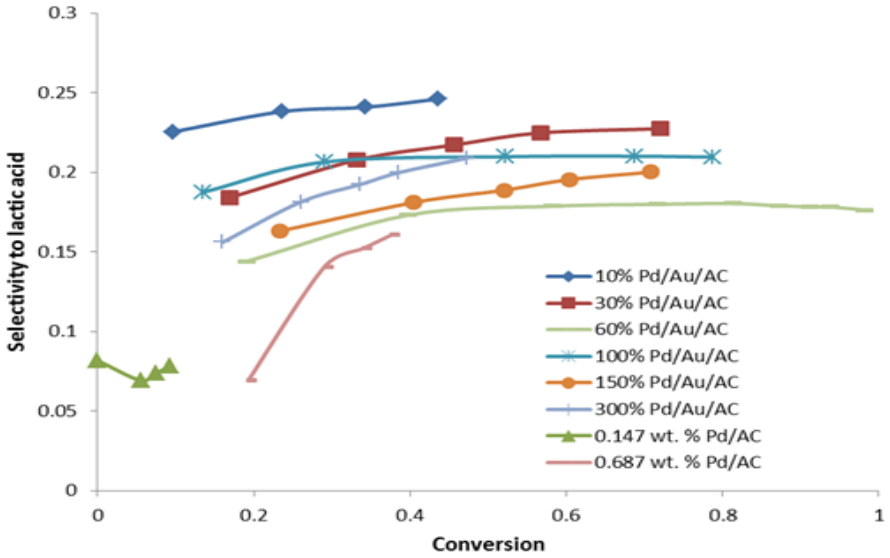


*Figure 22: Selectivity of lactic acid vs. conversion of glycerol*

### 2.5.4 Proposed reaction mechanism

Based on the reaction profiles (Figure 17 & 18), a reaction mechanism has been proposed (Figure 23).

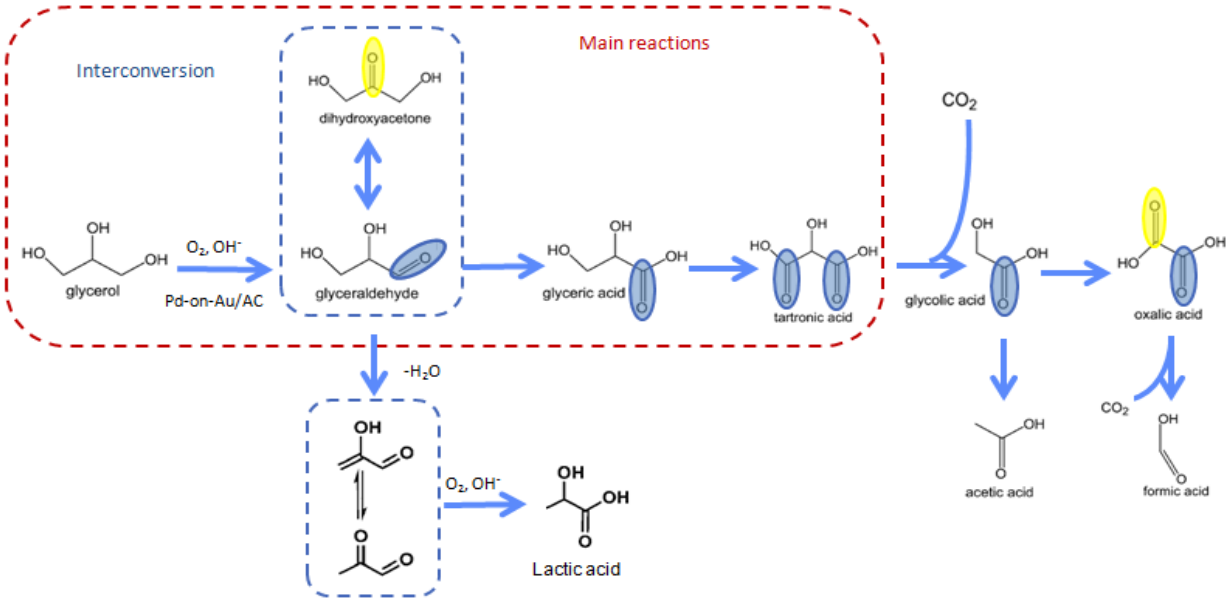


***Figure 23: Proposed reaction mechanism for liquid phase glycerol oxidation (yellow circle represents site oxidized from secondary OH group of glycerol; blue circle from primary OH group)***

It has been widely acknowledged that under high pH, glycerol is activated by scissoring the hydrogen from one of its primary hydroxyl groups to form glycerolate, which can be readily oxidized to glyceraldehyde on the catalyst surface [2,60]. Formed glyceraldehyde interconverts with dihydroxyacetone through carbonyl group rearrangement. However, dihydroxyacetone, its oxidized products and glyceraldehyde are very rarely reported as they are unstable under most experimental conditions (high pH and temperature). Interestingly, glyceraldehyde was always observed in a relatively large amount by Carrettin *et al.* [2]. This might be due to the experimental conditions used that were in

favor of the stability of glyceraldehyde, while others' did not.
The majority of glyceraldehyde is selectively oxidized into glyceric acid, which is a very stable compound and was found to be the major product by this study and by most other studies using Pd and Au catalysts. A competitive pathway of glyceraldehyde conversion to glyceric acid ascribes to the formation of lactic acid which was detected as the secondary major product in this study. Both Ketchie *et al.*[41] and Shen *et al.*[23] reported the formation of lactic acid in their works by using Au/C and Au-Pt/$TiO_2$ respectively. By controlling the experimental conditions, Shen *et al.* were able to achieve a 85.6% selectivity to lactic acid with high catalytic activity (TOF 517.1 $h^{-1}$). The formation of lactic acid was attributed to a base-catalyzed dehydration and benzilic acid rearrangement of glyceraldehyde intermediate as shown in Figure 23 [23].
With the other primary OH group oxidized, glyceric acid can be sequentially converted into tartronic acid which was the third major product. However, two side carboxylic groups with one hydroxyl group in the middle subject tartronic acid to C-C bond cleavage, resulting in the formation of glycolic acid, oxalic acid and carbon dioxide. David *et al.* examined the $H_2O_2$ formation during the reaction with Pd, Au, Pd-Au catalysts. They found that $H_2O_2$ contributed to the cleavage of C-C bond, thus detrimental to the selectivity towards glyceric acid. However, Pd was proposed to catalyze the decomposition of $H_2O_2$ that formed on both the Pd and Au surfaces, giving rise to a higher selectivity of using bimetallic catalyst [41, 60-61]. We validate this finding with the observation of higher selectivity to glyceric acid for Pd and Pd/Au catalysts.
Glycolic acid can also be oxidized into oxalic acid. Oxalic acid can subsequently undergo C-C bond cleavage to form formic acid. Acetic acid is also detected in the product mixture. The formation of it is proposed to be due to a reduction of the hydroxyl group of glycolic acid. The over-oxidation of formic acid and acetic acid is also thought to be responsible for the $CO_2$ formation. The reaction from glycerol to glyceric acid and to lactic acid with glyceraldehyde as intermediate and further to tartronic acid is the major reaction pathway, with $C_2$ and $C_1$ only existing in non-significant amounts.

### 2.5.5 Discussion

By depositing Pd onto a Au surface, both high resistance to deactivation from Au and high selectivity from Pd were maintained. Even for a Pd surface coverage at full monolayer coverage, Pd/Au can still keep its high activity and selectivity without any significant trace of deactivation.
In the HDC of TCE, mild reaction conditions were used (room temperature, atmospheric pressure), under which the oxidized surface of the monometallic Pd nanoparticles was not reduced. Thus, the metallic Pd atoms of the Pd/Au nanoparticles are suggested to be active sites for the room temperature aqueous-phase HDC reaction of TCE. Au nanoparticles appear to have a unique ability to stabilize surface Pd atoms in metallic form, possibly leading to a set of high active sites that is not present in monometallic Pd nanoparticles under ambient-temperature reaction conditions [6]. Since a similar volcano-shaped relationship between activity and Pd surface coverage was observed for glycerol oxidation, and for a typical selective oxidation reaction of glycerol, the temperature and pressure are very mild (60 °C 0.12 L/min $O_2$ flow). It can be hypothesized that the unique ability of Au on Pd should partially hold for glycerol oxidation, if not fully due to an oxidative environment. Based on this, the following hypothesis is proposed.
Metallic Pd ($Pd^0$) is very active in glycerol oxidation while oxidized Pd ($Pd^{2+}$) is much less active. ~4 nm Pd nanoparticles supported on AC catalyst have its Pd surface nearly 100% oxidized with a small proportion still in the metallic state which contributes to the

fast reaction rate initially. However, during the course of reaction, metallic Pd is gradually preoccupied by dissolved $O_2$ and oxidized to exhibit a deactivation pattern.
Pd/Au catalyst with a 60% Pd surface coverage has a Au rich core and Pd rich shell and its exposed surface consists of 40% Au atoms with 100% of them in metallic state and 60% Pd atoms with 70% of them in metallic state. $Pd^0$ contributes more to the activity and selectivity than $Au^0$. During the course of reaction, the metallic state of Pd is strongly maintained by metallic Au, enabling the reaction in high activity and selectivity. Although a small proportion of $Pd^0$ can still be oxidized, its resistance to deactivation is severely eliminated.

## *2.6 Conclusions*

Glycerol can be used as a raw material for synthesizing more functionalized and valuable products, such as glyceric acid, tartronic acid and lactic acid. AC supported monometallic Au and Pd catalysts and a series of Pd/Au catalysts with various Pd surface coverages have been tested in the liquid phase selective oxidation of glycerol. By addition of a Pd surface, bimetallic Pd/Au catalysts had both enhanced catalytic activities and selectivities towards glyceric acid over monometallic catalysts. Au and Pd catalysts were found to have similar selectivities to glyceric acid as Pd/Au catalysts but had much lower TOFs. Catalytic activity and selectivity of bimetallic Pd/Au catalysts were also found to be a function of surface coverage of the shell Pd atoms on the core Au atoms, with the highest activity and selectivity detected at ~60% and ~100% respectively. A 98.1% conversion of glycerol was observed at a 60% Pd surface coverage, in 3 hours time. It is hypothesized that the reactivity order for metal species is $Pd^0 > Au^0 > Pd^{2+}$ and Au has a unique ability to stabilize surface Pd atoms in metallic form that is resistant to experimental conditions (pH 13.6, 60 °C, and $O_2$ flow). This catalyst material provides a potential way to convert glycerol into more economically valuable products.
Results from different studies as described in Chapter 1.4.6 cannot be compared as such because of being derived under different reaction conditions (i.e. pressure, temperature, NaOH-glycerol ratio, amount and type of catalyst etc.).

## *2.7 Future work*

This thesis is the first chapter in the testing of the aqueous phase oxidation of glycerol mediated with a supported Pd-on-Au catalyst with varying Pd surface coverages. The objective was to gain more insight in the nanoscale Pd-on-Au catalyst and the reaction mechanism and kinetics of glycerol and its components in the selective oxidation reaction.

Further research can be done with the following:

- In this study a ~4 nm catalyst has been used. Varying the size of the catalyst could result in improved performance of the catalyst. In part II of this thesis some tests have been carried out with different sized catalysts;

- The structure of the catalyst could be affected during the reaction. The stability of the catalysts structure during the selective oxidation of glycerol can be determined by EXAFS (Extended X-ray Absorption Fine Structure). In part II of this thesis it has been investigated;

- To confirm the stability of the Pd-on-Au surface coverage and to rule out possible leaching, ICP-AES studies are necessary;

- During this study there were indications of $O_2$ poisoning of the catalyst. This has to be investigated further to confirm beyond doubt whether or not this is happening. If proven right, measures to prevent/reverse the $O_2$ poisoning should be researched;

- This study was performed in lab-scale and used pure $O_2$. However for up-scaling/industrial purposes the use of air instead of $O_2$ should be investigated. This could results in potential savings, reduced change of $O_2$ poisoning and less corrosion issues;

- During the experiments a temperature of 60°C was applied as this was mostly used in literature. However, repeating the experiments from this work at different temperatures could potentially improve the effectiveness of this catalytic process;

- NaOH was used as the base in the reactions with a ratio to glycerol of 4:1 (from literature studies). Varying the ratio and or replacing NaOH with another alkali could potentially enhance the performance of the process;

- The experiments performed used laboratory grade glycerol. For up-scaling purposes, the experiments need to be repeated using industrial grade glycerol;

- In this study, the experiments were performed in batch mode. The possibility of performing this reaction in continuous mode should be researched for possible industrial applications.

# 3 Part II – Study of stability in atomic-scale structure of supported palladium-on-gold catalysts with different core diameters during the aqueous-phase oxidation of glycerol

There are already over 800 everyday commercial products that rely on nanoscale materials and processes i.e. platinum nanoparticles are being used as catalytic reformers in petroleum refining improving the efficiency of fuel production [71]. Chemical catalysis benefits from nanoparticles due to their dramatically increased surface area to volume ratio. When using nanoparticles a greater amount of the active material of the catalyst comes in contact with the surrounding gas or liquid phase, thus affecting the reactivity.

Zheng *et al.* studied the size effects of Pt/C catalysts on the activity and selectivity of base-free glycerol oxidation. They observed that bigger Pt particles (>10 nm) were less active, an increase in glycerol conversion was found with a decrease in size (<6 nm). However, an increase in the selectivity to glyceric acid was found with larger Pt particles [71]. Prati *et al.,* Davis *et al.* and Claus *et al.* studied the size effects of Au catalysts on the activity and selectivity of glycerol oxidation. Prati *et al.* tuned the metal (Pd, Au, Pd-Au) particle size from 2 to 16 nm. They observed a progressive decrease of activity and simultaneously an increase in the selectivity to glyceric acid with larger particle sizes [51]. Davis *et al.* likewise found that 5 nm Au particles gave a TOF nearly an order of magnitude greater than the larger unsupported Au nanoparticles (>20 nm). However, larger Au particles were more selective to glyceric acid [41]. Claus *et al.* prepared Au/C catalysts with Au particle sizes in the range from 2 to 45 nm. In accordance with Prati's and Davis' work, a decrease of activity and an increase in the selectivity to glyceric acid was observed with larger Au nanoparticles [46]. It can be concluded that in overall a decrease in activity and increase in selectivity to glyceric acid is found with larger metal particle sizes. These experiments indicate clearly that the glycerol oxidation is structure-sensitive.
The interesting scientific and technological challenge associated with the use of nanoparticles as catalyst is the understanding of how the composition and atomic-scale structure of nanoparticles produce the best catalytic activity. Even though various studies have demonstrated the influence of the (gold) particle size on the catalytic performances in the reaction of glycerol oxidation, it seems that there is no general consensus about the mechanism.

In this work, the stability of supported Pd/Au nanoparticles with a core diameter of ~3, ~7 and ~10 nm with a Pd loading of 60% was determined by EXAFS. The stability in composition and atomic-scale structure of the catalysts in the liquid phase oxidation of glycerol in water using oxygen as the oxidant are reported.
Not tested were the selectivity to glyceric acid and overall activity of the catalysts in the glycerol oxidation reaction. This due to the fact that the catalysts used have different wt.% Pd and Au than the catalysts used in part I, this is required for the EXAFS analysis.

## *3.1 Hypothesis*

The following hypothesis is proposed, for Pd/Au bimetallic catalysts with respect to their composition and atomic-scale structure in liquid phase oxidation of glycerol:

- The structure of Pd/Au nanoparticles [6] holds for different core diameters and remains intact during the aqueous-phase selective oxidation of glycerol.

## 3.2 Catalyst preparation

Au nanoparticles of ~3, ~7 and ~10 nm are synthesized through a sodium citrate-tannic acid reduction method[6]. The different sizes Au nanoparticles were prepared as described in Chapter 2.2.1. However, to prepare Au nanoparticles with different diameters, various compositions of the reducing mixture should be used as shown in Table 7.

***Table 7: Composition of reduction mixture for various sized Au nanoparticles***

| Diameter/nm | Cit sol/ml | TA sol/ml | $K_2CO_3$ sol/ml | $H_2O$/ml |
|---|---|---|---|---|
| ~3 | 4 | 5 | 5 | 6 |
| ~7 | 4 | 0.5 | 0 | 15.5 |
| ~10 | 4 | 0.1 | 0 | 15.9 |

The more tannic acid used, the smaller the size of the particles, and vice versa. When the amount of TA sol is greater than 1 ml, a same amount of $K_2CO_3$ sol will have to be used to stabilize the pH at around 7.5-8.
Au nanoparticles in the final fluid were about 3, 7 and 10 nm in diameter according to TEM (Figure 24).

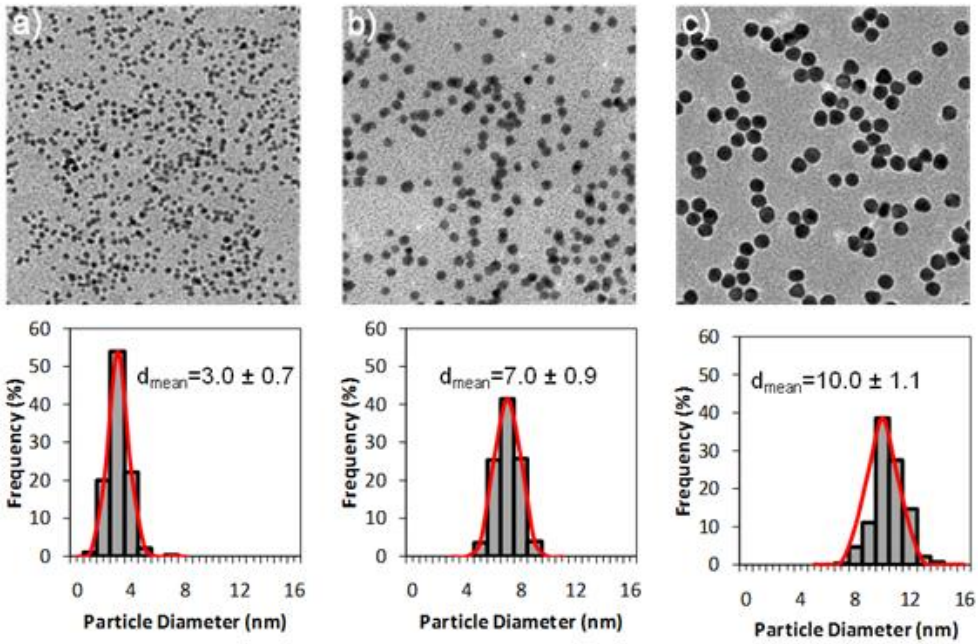


***Figure 24: TEM images and particle size distributions for a) ~3 nm Au nanoparticles b) ~7 nm Au nanoparticles and c) ~10 nm Au nanoparticles (courtesy of Lori Pretzer)***

To obtain the desired amounts of catalyst needed for the experiments, several batches of Au nanoparticles have to be prepared. For the ~3nm nanoparticles 6 batches, for the ~7nm nanoparticles 16 batches and for the ~10nm nanoparticles 22 batches of 100 mL have to be prepared.

### 3.2.1 Preparation of different sized bimetallic Pd/Au nanoparticles

In part I it was found that catalytic activity and selectivity of bimetallic Pd/Au catalysts in the oxidation of glycerol, were a function of surface coverage of the shell Pd atoms on the core Au atoms. The highest activity and selectivity were detected at ~60% and ~100% respectively. Also, in the HDC of TCE, the highest reaction rate was found with

[6] Described in Chapter 2.2.5

~4 nm Pd/Au nanoparticles at 60-70% Pd coverage [9]. Therefore, for the ~3, ~7 and ~10 nm Au nanoparticles, a 60% Pd surface coverage is used. The Pd was deposited on the Au nanoparticles as described in Chapter 2.2.2. Bimetallic Pd/Au nanoparticles were prepared by reducing Pd precursor in the preformed Au nanoparticles sol with hydrogen. Utilizing the magic cluster model, the amount of palladium solution needed to add for a 60% surface coverage on the different sized Au nanoparticles is calculated [6, 9] as shown in Table 8.

***Table 8: Amount of Pd solution needed for a 60% surface coverage for various sized Au nanoparticles***

| Diameter/nm | $PdCl_4$/ml |
|---|---|
| ~3 | 8.08 |
| ~7 | 2.93 |
| ~10 | 2.12 |

Table 8 shows that the amount of Pd precursor is less for larger particle sizes, which might seem peculiar. However, when preparing the Au nanoparticles, the precursor $HAuCl_4$ is always the same. Hereby, the total Au concentration is always the same for each of the syntheses. Therefore, with larger Au nanoparticles, there is less catalyst, which leads to lower amounts of Pd needed to acquire a 60% Pd surface coverage. For all catalyst sizes 1.0 wt.% Pd is used, this is necessary to get a good signal (in transmission mode) from the EXAFS[7].

### 3.2.2 Preparation different sized activated carbon supported Pd/Au catalysts

To prepare Pd/Au with 1.0 wt.% Pd supported on AC catalysts, 0.6 g of AC (Vulcan XC-72, Cabot) was added into 0.6 L of ~3 nm Pd/Au nanoparticle sol, 1.6 L of ~7 nm Pd/Au sol and 2.2 L of ~10 nm Pd/Au sol, and stirred vigorously for 12 hrs. After which all were centrifuged in batches at 14000 rpm under 4 °C for 40 min. The carbon slurry was collected and dried overnight in a vacuum oven at 60 °C to fully remove moisture. The catalyst was then crushed into powder for storage and catalytic testing. For each size, the catalyst powder was divided into three samples, one to be analysed as-prepared, one at the beginning of the glycerol oxidation reaction and one after. This is necessary to compare the final results and test whether the structure of Pd/Au nanoparticles remains intact during the aqueous-phase selective oxidation of glycerol. By preparing the catalysts at once and dividing it by three, all samples started the same.

## *3.3 Catalytic tests – selective oxidation reaction of glycerol – different sized catalyst*

Before the catalytic test, 0.2 grams[8] of each size catalyst are set aside for EXAFS characterization. These are the 'as-prepared' samples.
The aqueous-phase oxidation of glycerol with different sized catalysts was performed as described in Chapter 2.3. All experimental conditions were the same besides for the amounts of glycerol and NaOH used. Due to the higher Pd loading, a higher amount of glycerol is needed. Instead of 0.1M glycerol and 0.4M NaOH, 0.5M glycerol and 2M NaOH is used, the NaOH/glycerol molar ratio remains 4:1. Also, where in Part I the first sample was taken, the reaction is stopped by putting the reactor in an ice bath and

[7] Described in Appendix D
[8] Minimum amount required for EXAFS

purging it with $N_2$ for 5 min. After which the content of the reactor is centrifuged at 14000 rpm under 4 °C for 30 min. Subsequently, the excess water is removed by pipette. Next, the catalyst is washed by adding Nanopure water in the centrifuge tube. Thereafter the mixture is centrifuged again at 14000 rpm under 4 °C for 30 min. This is repeated once more after which the catalyst is dried and crushed. These are the 'at the beginning of the reaction' samples.
For the 'after the reaction' samples, the aqueous-phase oxidation of glycerol with different sized catalysts was performed fully as in Part I. After which the reaction is stopped and the catalyst is washed in the same manner as the 'during reaction' samples.

## *3.4 Method of analyzes (EXAFS)*

The as-prepared, at the beginning and after the reaction samples are dry black powders. These samples are analyzed by Extended X-ray Absorption Fine Structure (EXAFS) with courtesy of L. Pretzer and Z.Zhao.
The basic principle of XAFS is explained in Appendix E.
Measurements were carried out on the insertion-device beamline 10-ID-B of the Materials Research Collaborative Access Team (MRCAT) at the Advanced Photon Source at Argonne National Laboratory. A cryogenically cooled doublecrystal Si (1 1 1) monochromator was used in conjunction with an uncoated glass mirror to minimize the presence of harmonics. The monochromator was scanned continuously during the measurements with data points integrated over 0.5 eV for 0.07 s per data point. Measurements were made in transmission mode with the ionization chambers optimized for the maximum current with linear response (~$10^{10}$ photons detected per second) using a mixture of nitrogen and helium in the incident X-ray detector and a mixture of ~20% argon in nitrogen in the transmission X-ray detector. A gold or palladium foil spectrum was acquired simultaneously with each measurement for energy calibration.
The nanoparticle/C samples were pressed into a cylindrical holder with a thickness chosen to give a total absorbance (μx) at the Au $L_{III}$ (11.918 keV) and Pd K (24.350 keV) edges of ca. 2.0, and an edge step (Δμx) of ca. 0.5. For both Au and Pd edge the samples were analyzed as-prepared in air at RT and also treated at 200 °C for 30 min in 4% $H_2$/He then purged by He and cooled to RT. All spectra were obtained at RT.

Experimental data of Pd and Au foil were used to determine the best fit of Debye–Waller factors (DWF) and amplitude reduction factors ($S_o$) for phase shifts and back-scattering amplitudes in the FEFF fitting [73]. Along with the bond distance for Au and Pd foil, these values were used for determining the Au–Pd and Pd–Au FEFF phase shifts and back-scattering amplitudes. Standard procedures based on the WINXAS97 software [73] were used to extract the data [74]. The coordination parameters were obtained by a least-square fit in *k*- and *R*-space of the nearest-neighbour, $k^2$-weighted Fourier transform (FT) data (*k*: photoelectron wave number). The data fitted equally well with both $k^1$ and $k^3$ weightings. The data was fitted with courtesy of Dr. Miller at Argonne National Laboratory.

## *3.5 Results*

The XANES spectra of the ~3nm Pd/Au 'at the beginning of the reaction' nanoparticles at the Au $L_{III}$ edge in air at RT and reduced at 200 °C (Figure 25) are identical (both spectra are on the figure). The intensity and shape of the XANES are different. Metallic

Au seldom shows change from Au foil, but as seen in the figure, these differ in several places indicating alloy formation with Pd.

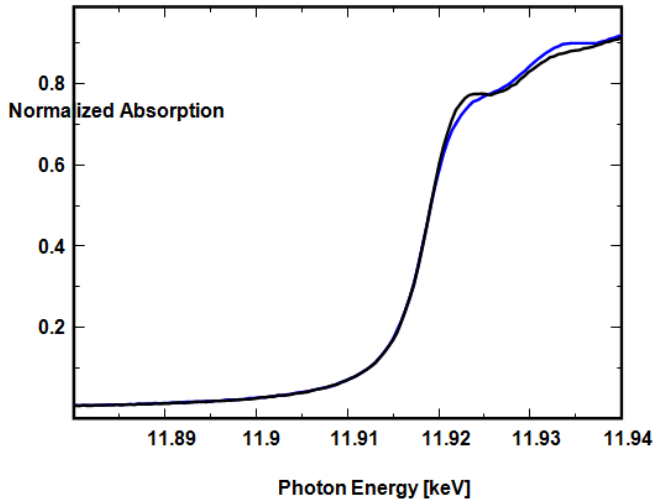


***Figure 25: XANES spectra of Au foil (black) at RT and ~3nm 'at the beginning of the reaction' Pd/Au nanoparticle/C at RT, and reduced at 200 °C (blue)***

The XANES spectra of the ~3nm Pd/Au 'at the beginning of the reaction' nanoparticles has a different shape than that of Pd foil (Figure 26). These changes are small since the electronic transition of the Pd K edge is a dipole forbidden electronic transition. The intensity of the air and reduced catalysts are identical and the same as Pd foil indicating fully reduced Pd atoms even in air.

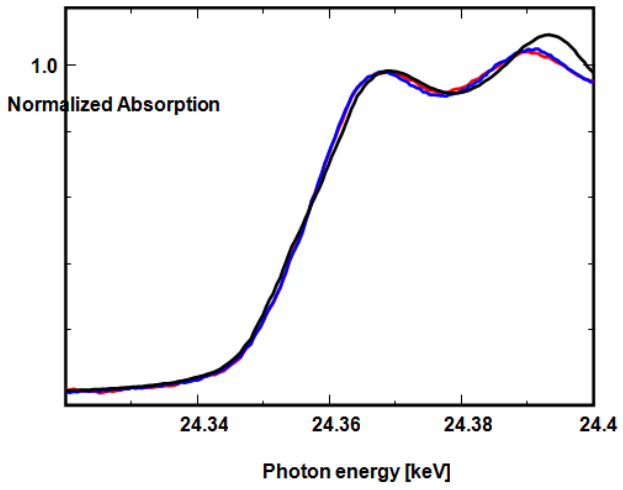


***Figure 26: XANES spectra of Pd foil (black) at RT and ~3nm 'at the beginning of the reaction' Pd/Au nanoparticle/C in air (red) at RT, and reduced at 200 °C (blue)***

The EXAFS of Pd/Au nanoparticles (Figure 27) are completely different from that of Pd foil indicating different neighbors, i.e., a high fraction of Pd with Au neighbors.

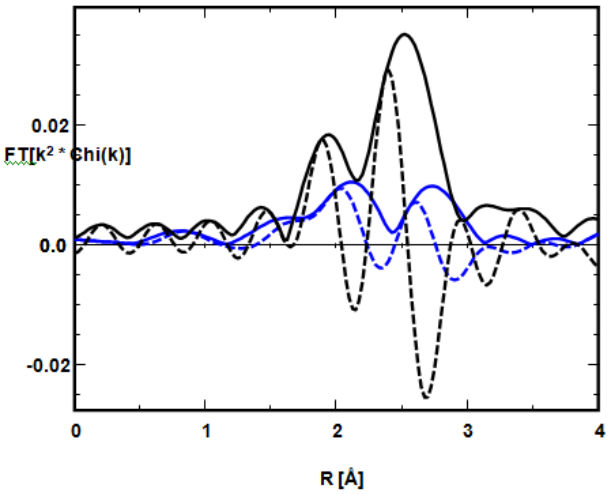


***Figure 27: Fourier transform (k² weighted, Δk = 2.6 – 10.5 Å$^{-1}$) of Pd K edge EXAFS for ~3nm 'at the beginning of the reaction' Pd/Au nanoparticle/C reduced at 200 °C (blue) and Pd foil (black): magnitude (solid) and imaginary components (dotted)***

Appendix F shows the results of EXAFS fitting. R is the bond distance in Angstrom (Å = $10^{-10}$m) between the central and neighboring atoms. For example, a Au-Pd bond distance of 2.74 Å means that the bond distance between the Au atom and Pd atom (from the perspective of the Au atom) is 2.79 Angstroms.
Within the error of the EXAFS measurements, bond distances for all samples remained constant during the reaction and also after RT treatment in air or after reduction at 200 °C. The Pd-Pd bond distance (2.74 Å) is similar to that in Pd foil (e.g., 2.75 Å). The Au-Au bond distance (2.85 Å) is slightly less than that of Au foil (2.88 Å), which is typical of nanoparticles. Also, the bond distances of Au–Pd ($R_{Au–Pd}$) and Pd–Au ($R_{Pd–Au}$) were identical at 2.79 Å.

The Debye-Waller Factor (DWF) is 0.0 with all measured samples.
The DWF is composed of thermal and static disorder. The DWF in the EXAFS fitting is the difference in disorder compared to a reference (Au foil & Pd foil). Therefore, a DWF of 0 means that the disorder is the same in the reference as it is in the sample. The DWF is also near 0 when having nanoparticles larger than about 7-8 nm. The DWF will increase when having smaller nanoparticles. The DWF will also increase when taking data at high T, which is due to thermal disorder. Finally, a DWF of 0 does not mean that there is no thermal or static disorder, it indicates it being very similar to that in foil, i.e., large particles.

N = coordination number (CN#) = the number of neighboring atoms
If for Au-Pd the CN# = 2.4, then each Au atom in each nanoparticle detects 2.4 Pd atoms on average. However, since 0.4 of an atom is not possible, the number is rounded down and it can be said that each Au atom detects ~2 Pd atoms. The structure of EXAFS is the average structure. Therefore, when having a mixture of particle morphologies, the average coordination number will be acquired.
The CN#s for all three nanoparticles sizes remains almost completely constant during the glycerol oxidation reaction. However, for the ~10nm nanoparticles, the Pd-Au CN# increases after being reduced at 200 °C and slightly increases during the oxidation reaction. This indicates that a small proportion of Pd has been oxidised.

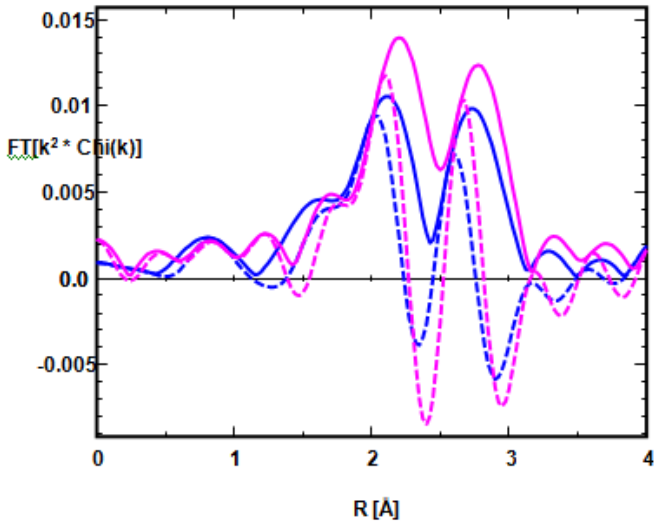


***Figure 28: Fourier transform (k² weighted, Δk = 2.6 – 10.5 Å⁻¹) of Pd K edge EXAFS for ~3nm 'at the beginning of the reaction' (blue) and ~10nm 'after the reaction' (pink) Pd/Au nanoparticles/C reduced at 200 °C: magnitude (solid) and imaginary components (dotted)***

As seen in Figure 28, the ~3nm 'at the beginning of the reaction' sample had more Pd-Pd neighbours than the ~10nm 'after the reaction' sample, which had very few. Which is logical since the sample is much smaller. Both had high Pd-Au coordination numbers which is consistent with the core–shell model in which Pd atoms are located on the surface of a Au-rich core. The differences in spectra are much smaller than between the Pd/Au nanoparticle and Pd foil (Figure 27). As the fraction of Pd-Au increases, the imaginary part moves to higher R (Pd-Au bonds are longer than Pd-Pd).

## *3.6 Conclusions*

Glycerol oxidation is structure-sensitive. Pd/Au nanoparticles with a core diameter of ~3, ~7 and ~10 nm with a Pd loading of 60% were prepared and characterized by EXAFS. The composition and atomic-scale structure of the catalysts in the liquid phase oxidation of glycerol in water using oxygen as the oxidant are reported. From the small change in Fourier transforms, the corresponding bond distances, the DWF of 0.0 and the almost completely constant CN#s, it can be concluded that the structure of Pd/Au nanoparticles holds for different core diameters and remains intact during the aqueous-phase selective oxidation of glycerol.

## *3.7 Future work*

This thesis is the first chapter in the testing of supported Pd-on-Au catalyst structure and size in the aqueous phase selective oxidation of glycerol. The objective was to gain more insight in the nanoscale Pd-on-Au catalyst structure and mechanism in the selective oxidation reaction.
Further research can be done with the following:

- Now that it is proven that the structure is persistent, the next step is to prepare Pd/Au/AC with 1.0 wt.% Au with different core diameters and test catalytic activity and selectivity in the aqueous-phase oxidation of glycerol;

- The size study can be expanded to even larger Pd/Au nanoparticles for structure analysis, to investigate whether the selectivity to glyceric acid can be further improved.

# References


1. J. Van Gerpen, B. Shanks and R. Pruszko, Biodiesel production technology, *NREL/SR-510-36244*, **2004**; http://www.nrel.gov/docs/fy04osti/36244.pdf
2. S. Carrettin, P. McMorn, P. Johnston, K. Griffin and G.J. Hutchings, *Chem. Commun.,* **2002**, 7, 696-697.
3. R. Garcia, M. Besson and P. Gallezot, *Appl. Catal. A-Gen.,* **1995**, 127, 165-176.
4. N. Dimitratos, F. Porta and L. Prati, *Appl. Catal. A-Gen.,* **2005**, 291, 210-214.
5. Y.L. Fang, J.T. Miller, N. Guo, K.N. Heck, P.J.J. Alvarez and M.S. Wong, *Catal. Today,* **2011**, 160, 96-102.
6. M.O. Nutt, J.B. Hughes and M.S. Wong, *Environ. Sci. Technol.,* **2005**, 39, 1346-1353.
7. M.S. Wong, P.J.J. Alvarez, Y.L. Fang, N. Akçin, M.O. Nutt, J.T. Miller and K.N. Heck, *J. Chem. Technol. Biot.,* **2009**, 84, 158-166.
8. M.O. Nutt, J.B. Hughes, M.S. Wong and W.M. Rice, *Abstr. Pap. Am. Chem. S.,* **2004**, 227, U1272.
9. M.O. Nutt, K.N. Heck, P. Alvarez and M.S. Wong, *Appl. Catal. B-Environ.,* **2006**, 69, 115-125.
10. K.N. Heck, B.G. Janesko, G.E. Scuseria, N.J. Halas and M.S. Wong, *Abstr. Pap. Am. Chem. S.,* **2008**, 235.
11. K.N. Heck, B.G. Janesko, G.E. Scuseria, N.J. Halas and M.S. Wong, *J. Am. Chem. Soc.,* **2008**, 130, 16592-16600.
12. R. Christoph, B. Schmidt, U. Steinberner and W. Dilla, Glycerol, *Ullmann's Encyclopedia of Industrial Chemistry,* **2000**.
13. J.N. Chheda, G.W. Huber and J.A. Dumesic, J.A., *Angew. Chem. Int. Edit.,* **2007**, 46, 7164-7183.
14. M. Pagliaro and M. Rossi, The Future of Glycerol: New Usages for a Versatile Raw Material, *ISSN:1757-7039*, RSC Publishing, Cambridge, **2008**.
15. B. Liu, Y. Zhang, J.W. Tierney and I. Wender, Hydrogen generation from glycerol via aqueous phase reforming, *CFFS Annual Meeting*, Daniels (WV), August 1, **2006**.
16. D.A. Simonetti, J. Rass-Hansen, E.L. Kunkes, R.R. Soares and J.A. Dumesic, *Green Chem.,* **2007**, 9, 1073-1083.
17. M.R. Nimlos, S.J. Blanksby, X. Qian, M.E. Himmel and D.K. Johnson, *J. Phys. Chem. A,* **2006**, 110, 6145-6156.
18. J.L. Dubois, C. Duquenne, W. Hoelderich and J. Kervennal, Process for dehydrating glycerol to acrolein, *EP1848681A2*, **2006**.
19. J. Chaminand, L. Djakovitch, P. Gallezot, P. Marion, C. Pinel and C. Rosier, *Green Chem.,* **2004**, 6, 359-361.
20. A. Behr and L. Obendorf, *Eng. Life Sci.,* **2002**, 2, 185-189.
21. S. Claude, Z. Mouloungui, J.W. Yoo and A. Gaset, Method for preparing glycerol carbonate, *US6025504*, **2000**.
22. M.A. Dasari, P.P. Kiatsimkul, W.R. Sutterlin and G.J. Suppes, *Appl. Catal. A-Gen.,* **2005**, 281, 225-231.
23. Y. Shen, S. Zhang, H. Li, Y. Ren and H. Liu, *Chem-Eur. J.,* **2010**, 16, 7368-7371.
24. M. Pagliaro, R. Ciriminna, H. Kimura, M. Rossi and C.D. Pina, *Angew. Chem. Int. Edit.,* **2007**, 46, 4434-4440.
25. Kimura, H., *Appl. Catal. A-Gen.,* **1993**, 105, 147-158.
26. H. Kimura, K. Tsuto, T. Wakisaka, Y. Kazumi and Y. Inaya, *Appl. Catal. A-Gen.,* **1993**, 96, 217-228.
27. P. Gallezot, *Catal. Today,* **1997**, 37, 405-418.

28. J.J. Berzelius, *Ann. Chim. Phys.*, **1836**, 61, 146-151.
29. K.J. Laidler, *Arch. Hist. Exact. Sci.,* **1986**, 35, 345-374.
30. H. Schmidbaur, *Naturwiss. Rundsch.,* **1995**, 48, 443-451.
31. G.C. Bond, P.A. Sermon, G. Webb, D.A. Buchanan and P.B. Wells, *J. Chem. Soc. Chem. Comm.,* **1973**, 444-445.
32. M. Haruta, T. Kobayashi, H. Sano and N. Yamada, *Chem. Lett.,* **1987**, 16, 405-408.
33. G.J. Hutchings, *J. Catal.,* **1985**, 96, 292-295.
34. B. Hammer and J.K. Norskov, *Nature,* **1995**, 376, 238-240.
35. B.N. Zope, D.D. Hibbits, M. Neurock and R.J. Davis, *Science*, **2010**, 330, 74-78.
36. A.S. K. Hashmi and G.J. Hutchings, *Angew. Chem. Int. Ed.,* **2006**, 45, 7896-7936.
37. M. Haruta, A. Ueda, R.M. Torres Sanchez and K. Tanaka, *Prp. Pet. Div. ACS Symp.,* New Orleans, **1996**.
38. S. Biella, G.L. Castiglioni, C. Fumagalli, L. Prati and M. Rossi, *Catal. Today,* **2002**, 72, 43–49.
39. M. Besson and P. Gallezot, *Catal. Today,* **2000**, 57, 127-141.
40. M. Comotti, C.D. Pina, R. Matarrese and M. Rossi, *Angew. Chem. Int. Ed.*, **2004**, 43, 5812-5815.
41. W.C. Ketchie, Y.L. Fang, M.S. Wong, M. Murayama and R.J. Davis, *J. Catal.,* **2007**, 250, 94-101.
42. L. Prati and M. Rossi, *J. Catal.,* **1998**, 176, 552-560.
43. C. Bianchi, F. Porta, L. Prati and M. Rossi, *Top. Catal.,* **2000**, 13, 231-236.
44. F. Porta, L. Prati, M. Rossi, S. Coluccia and G. Martra, *Catal. Today,* **2000**, 61, 165-172.
45. S. Carrettin, P. McMorn, P. Johnston, K. Griffin, C.J. Kiely and G.J. Hutchings, *Phys. Chem. Chem. Phys.,* **2003**, 5, 1329-1336.
46. S. Demirel-Gulen, M. Lucas and P. Claus, *Catal. Today,* **2005**, 102-103, 166-172.
47. S. Demirel, K. Lehnert, M. Lucas and P. Claus, *Appl. Catal. B-Environ.,* **2007**, 70, 637-643.
48. F. Porta and L. Prati, *J. Catal.,* **2004**, 224, 397-403.
49. N. Dimitratos, J.A. Lopez-Sanchez, J.M. Anthonykutty, G. Brett, A.F. Carley, R.C. Tiruvalam, A.A. Herzing, C.J. Kiely, D.W. Knight and G.J. Hutchings, *Phys. Chem. Chem. Phys.*, **2009**, 11, 4952-4961.
50. C.L. Bianchi, P. Canton, N. Dimitratos, F. Porta and L. Prati, *Catal. Today,* **2005**, 102-103, 203-212.
51. N. Dimitratos, J.A. Lopez-Sanchez, D. Lennon, F. Porta, L. Prati and A. Villa, *Catal. Lett.,* **2006**, 108, 147-153.
52. N. Dimitratos, C. Messi, F. Porta, L. Prati and A. Villa, *J. Mol. Catal. A-Chem.,* **2006**, 256, 21-28.
53. L. Prati, A. Villa, C. Campione and P. Spontoni, *Top. Catal.,* **2007**, 44, 319-324.
54. A. Villa, C. Campione and L. Prati, *Catal. Lett.,* **2007**, 115, 133-136.
55. D. Wang, A. Villa, F. Porta, L. Prati, and D. Su, *J. Phys. Chem. C,* **2008**, 112, 8617-8622.
56. N. Dimitratos, A. Villa and L. Prati, *Catal. Lett.,* **2009**, 133, 334-340.
57. R. Ciriminna and M. Pagliaro, *Adv. Synth. Catal.,* **2003**, 345, 383-388.
58. R.M. Painter, D.M. Pearson and R.M. Waymouth, *Angew. Chem. Int. Edit.,* **2010**, 49, 9456-9459.
59. W. Hu, D. Knight, B. Lowry and A. Varma, *Ind. Eng. Chem. Res.,* **2010**, 49, 10876-10882.
60. W.C. Ketchie, M. Murayama and R.J. Davis, *J. Catal.,* **2007**, 250, 264-273.
61. W.C. Ketchie, M. Murayama and R.J. Davis, *Top. Catal.,* **2007**, 44, 307-317.

62. T. Bligaard, J.K. Nørskov, S. Dahl, J. Matthiesen, C.H. Christensen and J. Sehested, *J. Catal.,* **2004**, 224, 206–217.
63. ATSDR, toxicological profile for tetrachloroethylene, *U.S. Department of Health and Human Services*, Public Health Service, Atlanta, GA: U.S., **1997**.
64. J.W. Slot and H.J. Geuze, *Eur. J. Cell Biol.,* **1985**, 38, 87-93.
65. S.K. Sivaraman, E. Iniyan, K. Sanjeev and S. Venugopal, *Curr. Sci. India.,* **2009**, 97, 1055-1059.
66. T. Ogata and Y. Nakano, *Water Res.,* **2005**, 39, 4281-4286.
67. J.M. Thomas, *Pure Appl. Chem.,* **1988**, 60, 1517-1528.
68. L.N. Lewis, *Chem. Rev.,* **1993**, 93, 2693-2730.
69. T. Teranishi and M. Miyake, *Chem. Mater.,* **1998**, 10, 594-600.
70. J.C. Slater, *J. Chem. Phys.,* **1964**, 41, 3199-3204.
71. The website for National Nanotechnology Initiative; http://www.nano.gov/you/nanotechnology-benefits
72. D. Liang, J. Gao, J. Wang, P. Chen, Z. Hou and X. Zheng, *Catal. Commun.,* **2009**, 10, 1586-1590.
73. T. Ressler, *J. Synchrotron Radiat.,* **1998**, 5, 118–122.
74. F.W. Lytle, D.E. Sayers and E.A. Stern*, Physica B,* **1989**, 158, 701–722.
75. G. Meitzner, *Catal. Today,* **1998**, 39, 281-291.
76. G. Vlaic, D. Andreatta and P.E. Colavita, *Catal. Today,* **1998**, 41, 261-275.
77. M. Newville, Fundamentals of XAFS, *Consortium for Advanced Radiation Sources,* University of Chicago, IL, **2004**, Revision 1.7.

# Appendices

## *Appendix A: Glycerol as building block for other chemicals [13]*

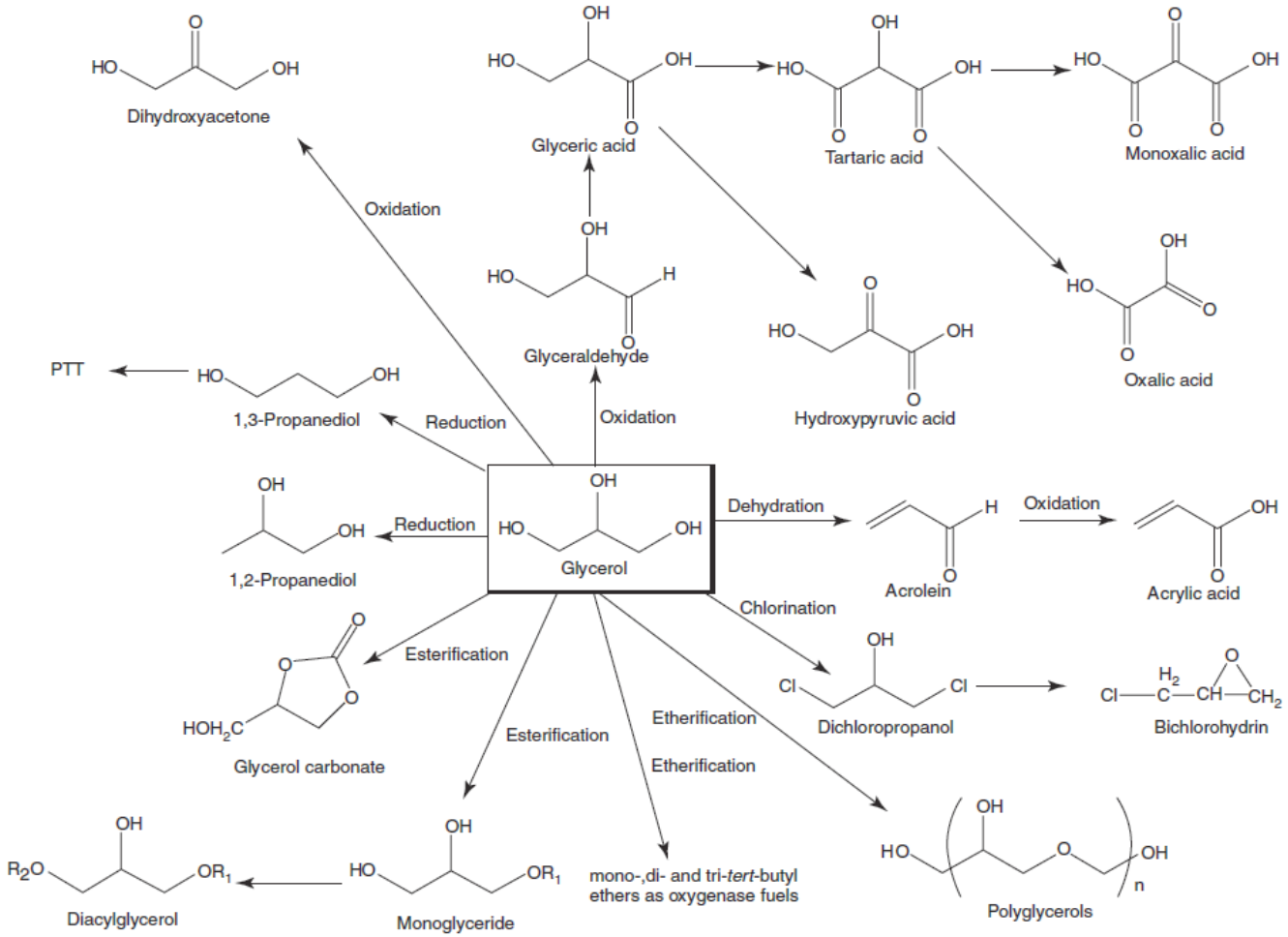

## *Appendix B: Effect of stirring rate*

The selective oxidation of glycerol using a supported catalyst is a typical solid-liquid-gas multiple phases reaction. The mass transfer includes gas-liquid transfer, liquid-solid transfer and intra-particle diffusion. A series of reactions with different stirring rates and catalyst amounts have been conducted to study the mass transfer effect during the reaction.

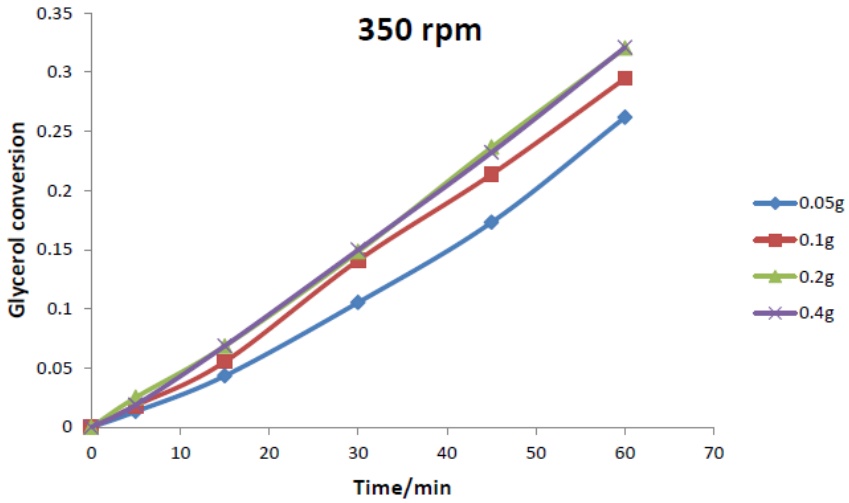


***Figure 29: Glycerol conversion at ~350 rpm using different amounts of catalyst (107 ml, 0.1 M glycerol, 0.4 M NaOH, 0.12 L/min $O_2$, 60 °C , 60% Pd/Au/AC)***

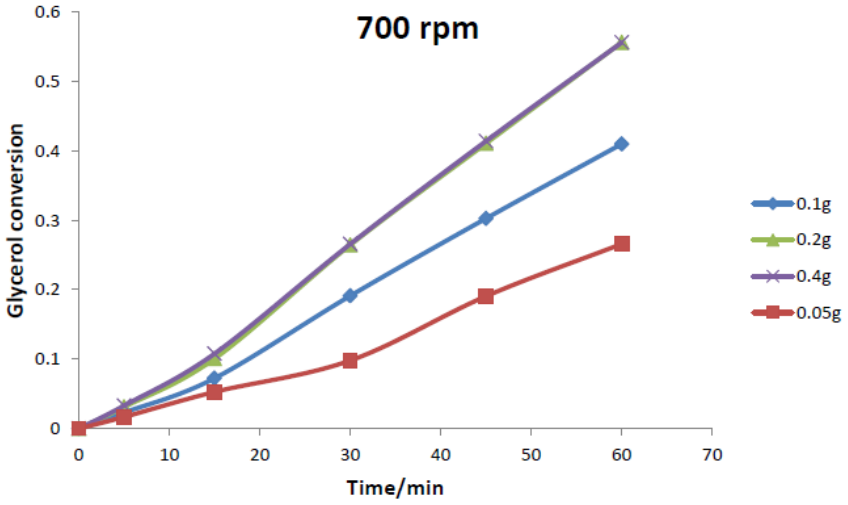


***Figure 30: Glycerol conversion at ~700 rpm using different amounts of catalyst (107 ml, 0.1 M glycerol, 0.4 M NaOH, 0.12 L/min $O_2$, 60 °C , 60% Pd/Au/AC)***

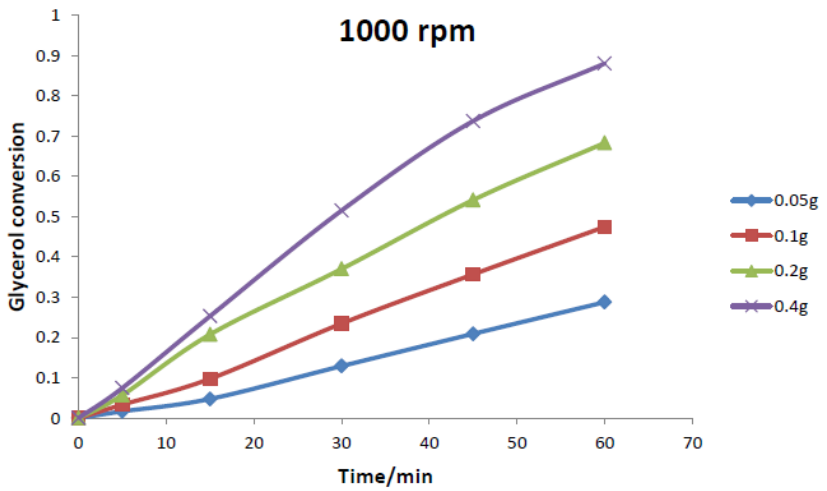


***Figure 31: Glycerol conversion at ~1000 rpm using different amounts of catalyst (107 ml, 0.1 M glycerol, 0.4 M NaOH, 0.12 L/min $O_2$, 60 °C , 60% Pd/Au/AC)***

From the results, we can clearly see that the stirring rate has a large effect on the observed catalytic activity. While keeping the amount of catalyst constant, a faster reaction occurred with a higher stirring rate. From this it can be concluded that with a higher stirring rate there is an increased gas-liquid/liquid-gas mass transfer.
As to the effect of catalyst amount; a higher amount of catalyst does not always mean an increased reactivity. The conversion profiles for 0.2 g and 0.4 g catalyst were almost identical with ~350 rpm (Figure 29) and also with ~700 rpm Figure 30), indicating that the mass transfer was a rate limiting. However, with a stirring rate of ~1000 rpm (Figure 31), the reaction was found to be much faster with 0.4 g catalyst than when using 0.2 g catalyst. In this operating region, mass transfer and surface reaction were comparable.

# *Appendix C: Catalysts information and reaction rate constants*

| Entry | Catalyst | Metal loading wt% | | Glycerol/metal mol ratio | | Glycerol conversion ( at 3h) in % | Reaction rate constants | | |
|---|---|---|---|---|---|---|---|---|---|
| | | *Au* | *Pd* | *Glycerol : Au* | *Glycerol : Pd* | | $K_{obs}$ ($h^{-1}$) | $k_{cat}$ ($L/g_{metal}/h$) | *Initial TOF (mol-glycerol/mol-$Pd_{surf}$/h)* |
| 1 | AC as received | 0 | 0 | - | - | 0 | 0 | 0 | 0 |
| 2 | AC as processed | 0 | 0 | - | - | 0 | 0 | 0 | 0 |
| 3 | Au/AC | 1 | 0 | 985:1 | - | 36.1 | 0.1423 | 7.7 | 439 |
| 4 | 10% Pd/Au/AC | 1 | 0.025 | 985:1 | 21284:1 | 58.8 | 0.3005 | 16.0 | 899 |
| 5 | 30% Pd/Au/AC | 1 | 0.074 | 985:1 | 7191:1 | 72.0 | 0.4277 | 21.7 | 1208 |
| **6** | **60% Pd/Au/AC** | **1** | **0.147** | **985:1** | **3620:1** | **98.1** | **1.3928** | **66.1** | **3631** |
| 7 | 100% Pd/Au/AC | 1 | 0.245 | 985:1 | 2172:1 | 88.3 | 0.739 | 32.3 | 1746 |
| 8 | 150% Pd/Au/AC | 1 | 0.368 | 985:1 | 1446:1 | 70.8 | 0.4108 | 16.0 | 857 |
| 9 | 300% Pd/Au/AC | 1 | 0.735 | 985:1 | 724:1 | 47.3 | 0.2082 | 5.9 | 315 |
| 10 | 0.147 wt. % Pd/AC | 0 | 0.147 | - | 3620:1 | 13.0 | 0.032 | 11.7 | 397 |
| 11 | 0.687 wt. % Pd/AC | 0 | 0.687 | - | 775:1 | 37.6 | 0.1145 | 8.9 | 304 |

## *Appendix D: Selectivity and molecular balance for all the catalysts*

| Entry | Catalyst | Selectivity (%) at 30% conversion | | | | | | | Molecular balance (3h) % |
|---|---|---|---|---|---|---|---|---|---|
| | | Glyceric acid | Tartronic acid | Lactic acid | Glycolic acid | Oxalic acid | Acetic acid | Formic acid | |
| 1 | Au/AC | 42.6 | 11.4 | 19.0 | 17.7 | 2.0 | 7.2 | 0 | 88.8 |
| 2 | 10% Pd/Au/AC | 45.0 | 7.8 | 24.1 | 7.2 | 0.7 | 4.1 | 11.3 | 91.9 |
| 3 | 30% Pd/Au/AC | 50.5 | 8.3 | 22.5 | 6.4 | 0.6 | 2.8 | 11.3 | 88.2 |
| 4 | 60% Pd/Au/AC | 52.4 | 11.6 | 16.0 | 5.8 | 1.4 | 0.7 | 12.0 | 83.2 |
| 5 | 100% Pd/Au/AC | 55.6 | 7.5 | 20.8 | 6.8 | 1.0 | 0 | 10.2 | 84.9 |
| 6 | 150% Pd/Au/AC | 53.2 | 7.6 | 17.0 | 8.4 | 1.6 | 0 | 12.0 | 88.8 |
| 7 | 300% Pd/Au/AC | 47.4 | 9.0 | 18.6 | 9.0 | 2.4 | 0 | 13.3 | 96.1 |
| 8 | 0.147 wt. % Pd/AC | - | - | - | - | - | - | - | 98.1 |
| 9 | 0.687 wt. % Pd/AC | 52.0 | 10.4 | 14.5 | 8.1 | 2.3 | 0 | 12.4 | 96.3 |

## *Appendix E: Basic principle of XAFS*

X-ray absorption spectroscopy (XAS) is a powerful technique to acquire detailed structural and electronic information on metallic nanoparticles [5, 73, 7573, 76]. By analyzing the XAFS, information on the local structure and on the unoccupied electronic states can be acquired. The x-ray absorption spectrum is typically divided into two regimes: x-ray absorption near-edge spectroscopy (XANES) and extended x-ray absorption fine-structure spectroscopy (EXAFS). Though the two have the same physical origin, this distinction is convenient for the interpretation. XANES is strongly sensitive to formal oxidation state and coordination chemistry (e.g., octahedral, tetrahedral coordination) of the absorbing atom, while the EXAFS is used to determine the distances, coordination number, and species of the neighbours of the absorbing atom [77]. XAS, especially in the EXAFS region, has been applied for characterization of bimetallic nanoparticles for decades.
The intensity of an x-ray beam passing through a material of thickness t is given by the absorption coefficient μ:

$$I = I_0 e^{-\mu t}$$

where $I_0$ is the x-ray intensity hitting the material, t is the sample thickness, and I is the intensity transmitted through the material, as shown in Figure 32.

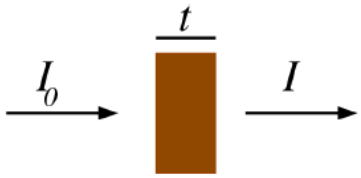


***Figure 32: General principle of a XAFS experiment [77]***

The x-ray intensity ($I_0$) is proportional to the number of x-ray photons.
The absorption coefficient μ depends strongly on x-ray energy E, atomic number Z, the density $\rho$ and atomic mass A:

$$\mu \approx \frac{\rho Z^4}{AE^3}$$

When the incident x-ray energy matches the binding energy of an electron of an atom within the sample, the number of x-rays absorbed by the sample increases dramatically, causing a drop in the transmitted x-ray intensity. This results in an absorption edge.
XAFS measures the energy dependency of the x-ray absorption coefficient μ(E) at and above the absorption edge of a selected element. The absorption coefficient can be measured two ways:

- Transmission: the absorption is measured directly by measuring what is transmitted through the sample

$$I = I_0 e^{-\mu(E)t}$$
$$\mu(E) = \log\left(I_0/I\right)$$

- Fluorescence: the re-filling the deep core hole is detected. Typically fluorescent x-ray is measured

$$\mu(E) \propto I_f / I_0$$

For concentrated samples, XAFS is best measured in transmission.

XAFS occurs because the photo-electron can scatter from a neighbouring atom. The scattered photo-electron can return to the absorbing atom, modulating the amplitude of the photo-electron wave-function at the absorbing atom. This in turn modulates the absorption coefficient, causing the EXAFS (Figure 33).

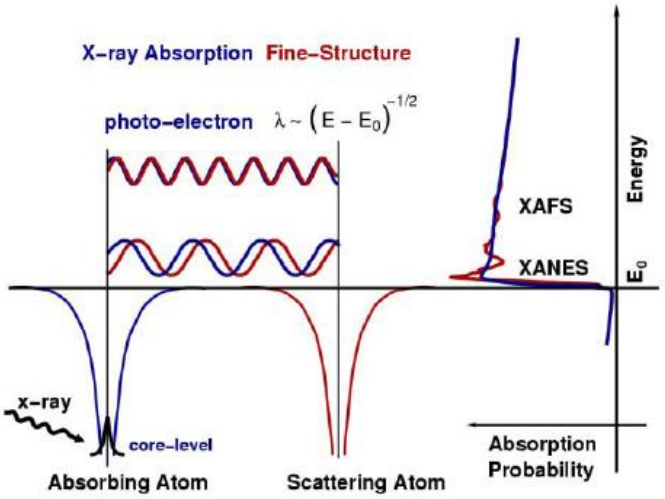


***Figure 33: Schematic representation of the mechanism of XAFS [77]***

To measure the absorption of a sample, a quite simple setup can be used (Figure 34).

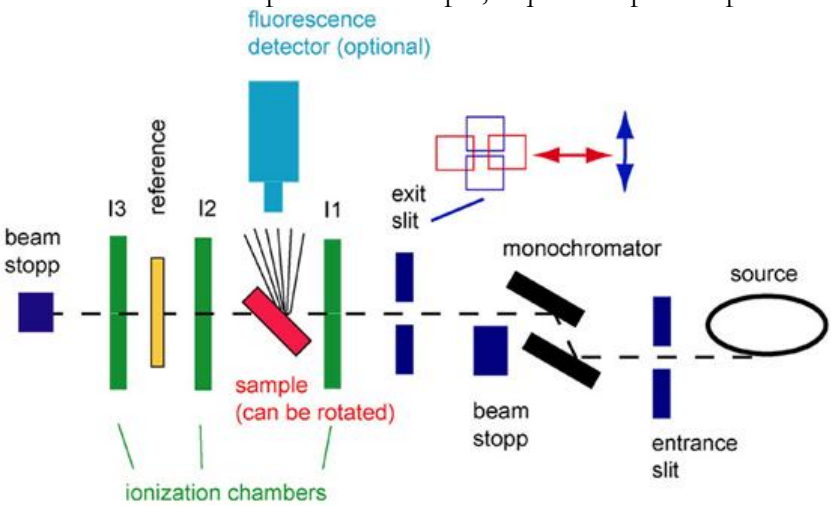


***Figure 34: Schematic XAFS experiment setup (Adapted from: http://www.desy.de)***

The photon beam from the synchrotron radiation source is first collimated by a slit system, i.e. sharp blades that can be adjusted to give a desired beam size. It is then passed to the double crystal monochromator, where a specific energy is selected. Afterwards, it passes

again a slit system. This has two reasons: On the one hand, the monochromator may broaden the beam due to surface defects of the crystals; on the other hand, the photon energy depends - as a result of Bragg's law - on the incident angle of the photon beam at the crystal. Although the beam has only little angular divergence, it might for this reason be useful to cut the beam further down to improve the energy resolution. After passing a first ionization chamber where the incoming intensity is measured, the photons hit the sample. A second ionization chamber measures the transmitted intensity. The absorption of the sample at a given energy may then be calculated by dividing the transmitted intensity by the incoming intensity (actually, what counts is the negative natural logarithm of this value).

**XAFS spectra**

The XAFS spectra are mainly recorded at the K-edge (and less frequently the L edges) of almost all the atoms with Z>3. The XANES region starts about 5 eV beyond the absorption threshold (Figure 35). Because of the low kinetic energy range (5-150 eV) the photoelectron backscattering amplitude by neighbor atoms is very large so that multiple scattering events become dominant in the XANES spectra.

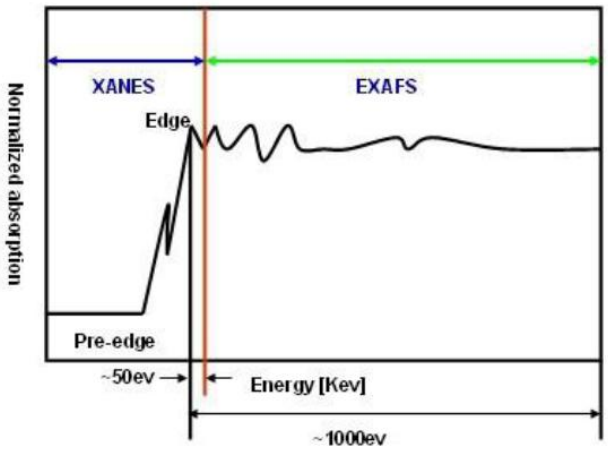


***Figure 35: A typical XAFS spectrum (Adapted from: UC Davis)***

EXAFS spectra are displayed as graphs of the absorption coefficient of a given material versus energy, typically in a 500-1000 eV range beginning before an absorption edge of an element in the sample (Figure 35). The x-ray absorption coefficient is usually normalized to unit step height. This is done by regressing a line to the region before and after the absorption edge, subtracting the pre-edge line from the entire data set and dividing by the absorption step height, which is determined by the difference between the pre-edge and post-edge lines at the value of $E_0$ (on the absorption edge).

**Data analysis**

No matter whether μ(E) is measured in transmission or fluorescence, the data reduction and analysis are essentially the same. The raw data is reduced by following steps: remove any instrumental background and absorption from other edges; identify the threshold energy $E_0$; normalize μ(E) to go from 0 to 1; remove a smooth post-edge background function to approximate $\mu_0(E)$; isolate the XAFS χ(k); k-weight the XAFS χ(k) and Fourier transform into R-space [77]. Figure 36 shows a Fourier transform magnitude components of Pd K edge EXAFS data.

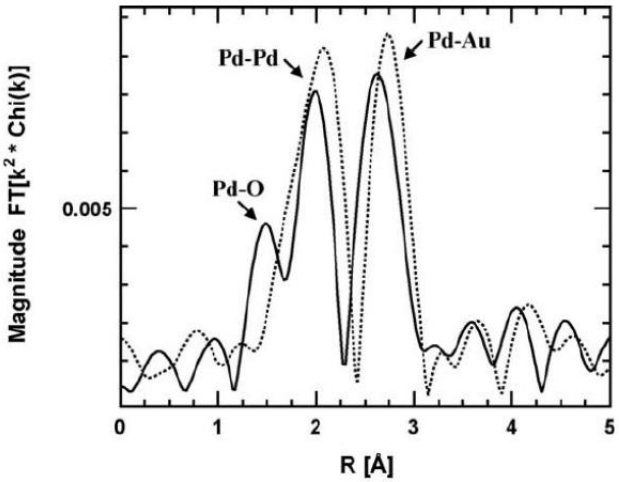


***Figure 36: Fourier transform magnitude components of Pd K edge EXAFS data for 0.6 mL Pd/Au nanoparticle/C: in air at RT (solid line), after reduced in $H_2$ at 300°C (dotted line)[5]***

The data gives direct evidence of bond information (distance, type, etc.). After being fit into the EXAFS equations, exact values for coordination numbers, bond distance, and oxidation state can be obtained.

***Appendix F: EXAFS fit parameters (N: coordination number; R: bond distance; DWF: Debye–Waller factor; $E_0$: threshold absorption edge energy)***

| Sample | Treatment | Scatter | N | R, Å | DWF (x $10^3$) | $E_0$, eV |
|---|---|---|---|---|---|---|
| B ~3nm | Air RT | Au-Au | 9.1 | 2.85 | 0.0 | 0.8 |
| | | Au-Pd | 2.4 | 2.79 | 0.0 | 2.7 |
| B ~3nm | $H_2$ 200C | Au-Au | 9.0 | 2.85 | 0.0 | 0.7 |
| | | Au-Pd | 2.6 | 2.79 | 0.0 | 2.0 |
| D ~3nm | Air RT | Au-Au | 9.2 | 2.85 | 0.0 | 0.4 |
| | | Au-Pd | 2.5 | 2.79 | 0.0 | 2.7 |
| D ~3nm | $H_2$ 200C | Au-Au | 9.1 | 2.85 | 0.0 | 0.8 |
| | | Au-Pd | 2.7 | 2.79 | 0.0 | 2.3 |
| A ~3nm | Air RT | Au-Au | 9.2 | 2.85 | 0.0 | 0.2 |
| | | Au-Pd | 2.7 | 2.79 | 0.0 | 1.9 |
| A ~3nm | $H_2$ 200C | Au-Au | 9.1 | 2.85 | 0.0 | 0.8 |
| | | Au-Pd | 2.9 | 2.79 | 0.0 | 2.4 |
| B ~7nm | Air RT | Au-Au | 10.3 | 2.85 | 0.0 | -0.6 |
| | | Au-Pd | 1.3 | 2.79 | 0.0 | 4.4 |
| B ~7nm | $H_2$ 200C | Au-Au | 10.0 | 2.85 | 0.0 | -0.4 |
| | | Au-Pd | 1.4 | 2.79 | 0.0 | 4.0 |
| D ~7nm | Air RT | Au-Au | 10.3 | 2.85 | 0.0 | -0.3 |
| | | Au-Pd | 1.3 | 2.79 | 0.0 | 4.5 |
| D ~7nm | $H_2$ 200C | Au-Au | 10.3 | 2.85 | 0.0 | -0.2 |
| | | Au-Pd | 1.4 | 2.79 | 0.0 | 3.4 |
| A ~7nm | Air RT | Au-Au | 10.3 | 2.85 | 0.0 | -0.4 |
| | | Au-Pd | 1.4 | 2.79 | 0.0 | 3.9 |
| A ~7nm | $H_2$ 200C | Au-Au | 10.3 | 2.85 | 0.0 | -0.1 |
| | | Au-Pd | 1.4 | 2.79 | 0.0 | 3.8 |
| B ~10nm | Air RT | Au-Au | 10.8 | 2.85 | 0.0 | -1.0 |
| | | Au-Pd | 1.1 | 2.79 | 0.0 | 6.7 |
| B ~10nm | $H_2$ 200C | Au-Au | 10.8 | 2.85 | 0.0 | -0.7 |
| | | Au-Pd | 1.1 | 2.79 | 0.0 | 5.8 |
| D ~10nm | Air RT | Au-Au | 10.8 | 2.85 | 0.0 | -0.9 |
| | | Au-Pd | 1.1 | 2.79 | 0.0 | 6.6 |
| D ~10nm | $H_2$ 200C | Au-Au | 10.8 | 2.85 | 0.0 | -0.5 |
| | | Au-Pd | 1.1 | 2.79 | 0.0 | 5.5 |
| A ~10nm | Air RT | Au-Au | 10.7 | 2.85 | 0.0 | -0.7 |
| | | Au-Pd | 1.1 | 2.79 | 0.0 | 6.1 |
| A ~10nm | $H_2$ 200C | Au-Au | 10.8 | 2.85 | 0.0 | -0.6 |
| | | Au-Pd | 1.2 | 2.79 | 0.0 | 5.5 |

| Sample | Treatment | Scatter | N | R, Å | DWF (x $10^3$) | $E_0$, eV |
|---|---|---|---|---|---|---|
| B ~3nm | Air RT | Pd-Pd | 2.2 | 2.74 | 0.0 | -7.1 |
| | | Pd-Au | 9.5 | 2.79 | 0.0 | -4.6 |
| B ~3nm | $H_2$ 200C | Pd-Pd | 2.1 | 2.74 | 0.0 | -6.5 |
| | | Pd-Au | 9.5 | 2.79 | 0.0 | -4.4 |
| D ~3nm | Air RT | Pd-Pd | 1.6 | 2.74 | 0.0 | -5.1 |
| | | Pd-Au | 8.9 | 2.79 | 0.0 | -4.3 |
| D ~3nm | $H_2$ 200C | Pd-Pd | 1.9 | 2.74 | 0.0 | -6.5 |
| | | Pd-Au | 10.0 | 2.79 | 0.0 | -4.4 |
| A ~3nm | Air RT | Pd-Pd | 1.7 | 2.74 | 0.0 | -6.5 |
| | | Pd-Au | 8.9 | 2.79 | 0.0 | -4.4 |
| A ~3nm | $H_2$ 200C | Pd-Pd | 1.9 | 2.74 | 0.0 | -6.4 |
| | | Pd-Au | 10.1 | 2.79 | 0.0 | -4.6 |
| B ~7nm | Air RT | Pd-Pd | 0.6 | 2.74 | 0.0 | -3.0 |
| | | Pd-Au | 9.8 | 2.79 | 0.0 | -5.9 |
| B ~7nm | $H_2$ 200C | Pd-Pd | 1.1 | 2.74 | 0.0 | 2.2 |
| | | Pd-Au | 10.2 | 2.79 | 0.0 | -6.4 |
| D ~7nm | Air RT | Pd-Pd | 0.6 | 2.74 | 0.0 | -3.8 |
| | | Pd-Au | 10.0 | 2.79 | 0.0 | -5.5 |
| D ~7nm | $H_2$ 200C | Pd-Pd | 0.7 | 2.74 | 0.0 | -4.0 |
| | | Pd-Au | 10.2 | 2.79 | 0.0 | -6.1 |
| A ~7nm | Air RT | Pd-Pd | 0.2 | 2.74 | 0.0 | -4.6 |
| | | Pd-Au | 9.8 | 2.79 | 0.0 | -6.6 |
| A ~7nm | $H_2$ 200C | Pd-Pd | 0.5 | 2.74 | 0.0 | -4.3 |
| | | Pd-Au | 10.9 | 2.79 | 0.0 | -6.2 |
| B ~10nm | Air RT | Pd-Pd | 0.6 | 2.74 | 0.0 | -6.5 |
| | | Pd-Au | 8.8 | 2.79 | 0.0 | -5.3 |
| B ~10nm | $H_2$ 200C | Pd-Pd | 1.0 | 2.74 | 0.0 | -6.4 |
| | | Pd-Au | 10.0 | 2.79 | 0.0 | -5.6 |
| D ~10nm | Air RT | Pd-Pd | 0.2 | 2.74 | 0.0 | -4.4 |
| | | Pd-Au | 8.6 | 2.79 | 0.0 | -6.2 |
| D ~10nm | $H_2$ 200C | Pd-Pd | 0.5 | 2.74 | 0.0 | -5.4 |
| | | Pd-Au | 10.5 | 2.79 | 0.0 | -5.6 |
| A ~10nm | Air RT | Pd-Pd | 0.1 | 2.74 | 0.0 | -4.2 |
| | | Pd-Au | 9.4 | 2.79 | 0.0 | -5.9 |
| A ~10nm | $H_2$ 200C | Pd-Pd | 0.1 | 2.74 | 0.0 | -5.3 |
| | | Pd-Au | 11.0 | 2.79 | 0.0 | -6.0 |

B - 'at the beginning of the reaction' samples
D - 'during reaction' samples
A - 'after the reaction' samples